

1 **Characterization of a Real-Time Tracer for Isoprene Epoxydiols-Derived Secondary**  
2 **Organic Aerosol (IEPOX-SOA) from Aerosol Mass Spectrometer Measurements**

3 Weiwei Hu<sup>1,2</sup>, Pedro Campuzano-Jost<sup>1,2</sup>, Brett B. Palm<sup>1,2</sup>, Douglas A. Day<sup>1,2</sup>, Amber M.  
4 Ortega<sup>1,3</sup>, Patrick L. Hayes<sup>1,2\*</sup>, Jordan E. Krechmer<sup>1,2</sup>, Qi Chen<sup>4,5</sup>, Mikinori Kuwata<sup>4,6</sup>, Yingjun  
5 Liu<sup>4</sup>, Suzane S. de Sá<sup>4</sup>, Karena McKinney<sup>4</sup>, Scot T. Martin<sup>4</sup>, Min Hu<sup>6</sup>, Sri Hapsari  
6 Budisulistiorini<sup>7</sup>, Matthieu Riva<sup>7</sup>, Jason D. Surratt<sup>7</sup>, Jason M. St. Clair<sup>8\*\*,\*\*\*</sup>, Gabriel Isaacman-  
7 Van Wertz<sup>9</sup>, Lindsay D. Yee<sup>9</sup>, Allen H. Goldstein<sup>9,10</sup>, Samara Carbone<sup>11</sup>, Joel F. de Brito<sup>11</sup>  
8 Paulo Artaxo<sup>11</sup>, Joost de A. Gouw<sup>1,2,12</sup>, Abigail Koss<sup>2,12</sup>, Armin Wisthaler<sup>13,14</sup>, Tomas  
9 Mikoviny<sup>13</sup>, Thomas Karl<sup>15</sup>, Lisa Kaser<sup>16,14</sup>, Werner Jud<sup>14</sup>, Armin Hansel<sup>14</sup>, Kenneth S.  
10 Docherty<sup>17</sup>, M. Elizabeth Alexander<sup>18</sup>, Niall H. Robinson<sup>19\*\*\*\*</sup>, Hugh. Coe<sup>19</sup>, James D. Allan<sup>19,20</sup>,  
11 Manjula R. Canagaratna<sup>21</sup>, Fabien Paulot<sup>22,23</sup>, and Jose L. Jimenez<sup>1,2</sup>.

12  
13 1 Cooperative Institute for Research in Environmental Sciences, University of Colorado,  
14 Boulder, CO, USA

15 2 Department of Chemistry and Biochemistry, University of Colorado, Boulder, CO, USA

16 3 Department of Atmospheric and Oceanic Sciences, University of Colorado, Boulder, CO, USA

17 4 School of Engineering and Applied Sciences and Department of Earth and Planetary Sciences,  
18 Harvard University, Cambridge, MA, USA

19 5 State Key Joint Laboratory of Environmental Simulation and Pollution Control, College of  
20 Environmental Sciences and Engineering, Peking University, Beijing, China

21 6 Earth Observatory of Singapore, Nanyang Technological University, Singapore 7 Department  
22 of Environmental Sciences and Engineering, Gillings School of Global Public Health, The  
23 University of North Carolina at Chapel Hill, Chapel Hill, NC, USA

24 8 Division of Geological and Planetary Sciences, California Institute of Technology, Pasadena,  
25 CA, USA

26 9 Department of Environmental Science, Policy, and Management, University of California,  
27 Berkeley, CA, USA

28 10 Department of Civil and Environmental Engineering, University of California, Berkeley, CA,  
29 USA

30 11 Department of Applied Physics, University of Sao Paulo, Sao Paulo, Brazil

31 12 NOAA Earth System Research Laboratory, Boulder, CO, USA

32 13 Department of Chemistry, University of Oslo, Oslo, Norway

33 14 Institute for Ion Physics and Applied Physics, University of Innsbruck, Innsbruck, Austria

34 15 Institute of Atmospheric and Cryospheric Sciences, University of Innsbruck, Innsbruck, Austria

35 16 Atmospheric Chemistry Division (ACD), National Center for Atmospheric Research,  
36 Boulder, CO, USA

37 17 Alion Science and Technology, Research Triangle Park, NC, USA

38 18 Environmental Molecular Sciences Laboratory, Pacific Northwest National Laboratory,  
39 Richland, WA, USA

40 19 School of Earth, Atmospheric and Environmental Sciences, University of Manchester, UK

41 20 National Centre for Atmospheric Science, University of Manchester, UK

42 21 Aerodyne Research, Inc., Billerica, MA, USA

43 22 NOAA Geophysical Fluid Dynamics Laboratory, Princeton, NJ, USA

44 23 Program in Atmospheric and Oceanic Sciences, Princeton University, Princeton, NJ, USA.

45 \*Now at: Department of Chemistry, Université de Montréal, Montréal, QC, Canada  
46 \*\* Now at: Atmospheric Chemistry and Dynamics Laboratory, NASA Goddard Space Flight  
47 Center, Greenbelt, MD, USA  
48 \*\*\* Now at: Joint Center for Earth Systems Technology, University of Maryland Baltimore  
49 County, Baltimore, MD, USA.  
50 \*\*\*\*\* Now at: Met Office, Exeter, UK  
51

## 52 Abstract

53 Substantial amounts of secondary organic aerosol (SOA) can be formed from isoprene  
54 epoxydiols (IEPOX), which are oxidation products of isoprene mainly under low-NO conditions.  
55 Total IEPOX-SOA, which may include SOA formed from other parallel isoprene oxidation  
56 pathways, was quantified by applying Positive Matrix Factorization (PMF) to aerosol mass  
57 spectrometer (AMS) measurements. The IEPOX-SOA fractions of OA in multiple field studies  
58 across several continents are summarized here and show consistent patterns with the  
59 concentration of gas-phase IEPOX simulated by the GEOS-Chem chemical transport model.  
60 During the Southern Oxidant and Aerosol Study (SOAS) study, 78% of PMF-resolved IEPOX-  
61 SOA is accounted by the measured IEPOX-SOA molecular tracers (methyltetrols, C5-Triols and  
62 IEPOX-derived organosulfate and its dimers), making it the highest level of molecular  
63 identification of an ambient SOA component to our knowledge. Enhanced signal at  $C_5H_6O^+$  ( $m/z$   
64 82) is found in PMF-resolved IEPOX-SOA spectra. To investigate the suitability of this ion as a  
65 tracer for IEPOX-SOA, we examine  $f_{C_5H_6O}$  ( $f_{C_5H_6O} = C_5H_6O^+/OA$ ) across multiple field, chamber  
66 and source datasets. A background of  $\sim 1.7 \pm 0.1\%$  ( $\%$ =parts per thousand) is observed in studies  
67 strongly influenced by urban, biomass-burning and other anthropogenic primary organic aerosol  
68 (POA). Higher background values of  $3.1 \pm 0.6\%$  are found in studies strongly influenced by  
69 monoterpene emissions. The average laboratory monoterpene SOA value ( $5.5 \pm 2.0\%$ ) is 4 times  
70 lower than the average for IEPOX-SOA ( $22 \pm 7\%$ ), which leaves some room to separate both  
71 contributions to OA. Locations strongly influenced by isoprene emissions under low-NO levels  
72 had higher  $f_{C_5H_6O}$  ( $\sim 6.5 \pm 2.2\%$  on average) than other sites, consistent with the expected IEPOX-  
73 SOA formation in those studies.  $f_{C_5H_6O}$  in IEPOX-SOA is always elevated (12–40%) but varies  
74 substantially between locations, which is shown to reflect large variations in its detailed  
75 molecular composition. The low  $f_{C_5H_6O}$  ( $< 3\%$ ) reported in non IEPOX-derived isoprene-SOA  
76 from chamber studies indicates that this tracer ion is specifically enhanced from IEPOX-SOA,  
77 and is not a tracer for all SOA from isoprene. We introduce a graphical diagnostic to study the  
78 presence and aging of IEPOX-SOA as a “triangle plot” of  $f_{CO_2}$  vs.  $f_{C_5H_6O}$ . Finally, we develop a  
79 simplified method to estimate ambient IEPOX-SOA mass concentrations, which is shown to  
80 perform well compared to the full PMF method. The uncertainty of the tracer method is up to a  
81 factor of  $\sim 2$  if the  $f_{C_5H_6O}$  of the local IEPOX-SOA is not available. When only unit mass  
82 resolution data is available, as with the aerosol chemical speciation monitor (ACSM), all  
83 methods may perform less well because of increased interferences from other ions at  $m/z$  82.  
84 This study clarifies the strengths and limitations of the different AMS methods for detection of  
85 IEPOX-SOA and will enable improved characterization of this OA component.

## 86 1. Introduction

87 Isoprene (2-methyl-1,3-butadiene, C<sub>5</sub>H<sub>8</sub>) emitted by vegetation is the most abundant non-  
88 methane hydrocarbon emitted to the Earth's atmosphere (~440–600 TgC/year) (Guenther et al.,  
89 2012). It is estimated to contribute substantially to the global secondary organic aerosol (SOA)  
90 budget (Paulot et al., 2009b;Guenther et al., 2012). Higher SOA yields from isoprene are  
91 observed under low-NO<sub>x</sub> conditions (Surratt et al., 2010). Under low-NO conditions, i.e. when a  
92 substantial fraction of the peroxy radicals do not react with NO, gas-phase isoprene epoxydiols  
93 (IEPOX) are produced with high yield through a HO<sub>x</sub>-mediated mechanism (Paulot et al.,  
94 2009b). Note that some IEPOX can also be formed from isoprene in high NO region via  
95 oxidation of the product 4-hydroxy-3-nitroso isoprene (Jacobs et al., 2014) , however this  
96 pathway is thought to be much smaller than the low-NO pathway. Subsequently, IEPOX can be  
97 taken up by acidic aerosols (Gaston et al., 2014), where IEPOX-SOA can be formed through  
98 acid-catalyzed oxirane ring-opening of IEPOX (Cole-Filipiak et al., 2010;Eddingsaas et al.,  
99 2010;Lin et al., 2012;Nguyen et al., 2014), which is thought to be the main pathway to form  
100 IEPOX-SOA (Surratt et al., 2010;Pye et al., 2013;Worton et al., 2013). Although the complete  
101 molecular composition of IEPOX-SOA has not been elucidated, several molecular species that  
102 are part of IEPOX-SOA have been identified through gas chromatography/mass spectrometry  
103 (GC/MS), liquid chromatography/mass spectrometry (LC/MS) and particle analysis by laser  
104 mass spectrometry (PALMS). They include 2-methyltetrols (and oligomers that contain them)  
105 (Surratt et al., 2010;Lin et al., 2014), C<sub>5</sub>-alkene triols (Wang et al., 2005), 3-  
106 methyltetrahydrofuran-3,4-diols (Lin et al., 2012), and an IEPOX-organosulfate (Froyd et al.,  
107 2010;Liao et al., 2014). These molecular species account for a variable fraction of the IEPOX-  
108 SOA reported, e.g., 8% in a chamber study (Lin et al., 2012) or 26% in a field study at Look  
109 Rock, TN (Budisulistiorini et al., 2015). An estimate of total IEPOX-SOA can also be derived

110 from an IEPOX-SOA molecular tracer(s) via multiplying the tracer concentration by the total  
111 IEPOX-SOA to tracer ratio. However, that method is hindered by the limited information on  
112 these molecular tracers and the reported variability of IEPOX-SOA to tracer ratios. IEPOX-SOA  
113 may include SOA formed from other parallel isoprene low-NO oxidation pathways (Liu et al.,  
114 2014; Krechmer et al. 2015). In addition, the IEPOX-SOA molecular tracers are typically  
115 measured with slow time resolution (12/24 h).

116 Multiple field studies, supported by chamber studies, have shown that the total amount of  
117 IEPOX-SOA can be obtained by factor analysis of organic spectra from an aerosol mass  
118 spectrometer (AMS) or the aerosol chemical speciation monitor (ACSM) (Robinson et al.,  
119 2011; Lin et al., 2012; Budisulistiorini et al., 2013; Nguyen et al., 2014). Robinson et al. (2011)  
120 first reported an SOA factor with pronounced  $f_{82}$  ( $= m/z$  82/OA) in the mass spectra acquired  
121 above a forest with high isoprene emissions in Borneo, and hypothesized that the elevated  $f_{82}$   
122 may have arisen from methylfuran ( $C_5H_6O$ ), consistent with  $C_5H_6O^+$  being the major ion at  $m/z$   
123 82 in isoprene-influenced areas. Lin et al. (2012) demonstrated that the 3-MeTHF-3,4-diols  
124 associated with IEPOX-SOA result in enhanced  $f_{82}$  in AMS spectra, presumably through the  
125 formation methylfuran-like structures during thermal desorption. Electron-impact ionization of  
126 aerosols formed by atomizing a solution containing IEPOX ( $C_5H_{10}O_3$ ) can also yield  $C_5H_6O^+$   
127 signals in an AMS via two dehydration reactions (Lin et al., 2012). However, because gas-phase  
128 IEPOX has high volatility, non-reactive gas-to-particle partitioning of IEPOX into OA is  
129 negligible under typical ambient concentrations in forest areas ( $1-10 \mu g m^{-3}$ ) (Worton et al.,  
130 2013).

131 IEPOX-SOA was estimated to account for 33% of ambient OA in summertime Atlanta from  
132 PMF analysis of ACSM spectra. The source apportionment result was supported by the

133 pronounced  $f_{82}$  peak in the factor spectrum and good temporal correlation of the factor with  
134 sulfate and 2-methyltetrols (Budisulistiorini et al., 2013). Sulfate is often strongly correlated with  
135 the acidity of an aerosol, and might also play a direct role in the chemistry, e.g. via direct  
136 reaction or nucleophilic effects (Surratt et al., 2007; Liao et al., 2014; Xu et al., 2014). While  
137 discussing the results of a recent aircraft campaign from Brazil, Allan et al. (2014) also used  $f_{82}$   
138 as a tracer for IEPOX-SOA.

139 If  $f_{82}$  in AMS spectra (and/or  $f_{C_5H_6O}$  in HR-AMS spectra) is dominated by IEPOX-SOA,  $f_{82}$   
140 would be a convenient, high-time-resolution, and potentially quantitative tracer for IEPOX-SOA.  
141 Thus, it will be very useful for investigating the impacts of SOA formation from isoprene with  
142 AMS/ACSM measurements, which have become increasingly common in recent years including  
143 some continental-scale continuous networks (Fröhlich et al., 2015). However, no studies to date  
144 have systematically examined whether enhanced  $f_{82}$  is unique to IEPOX chemistry or whether it  
145 could also be enhanced in other sources. Nor has the range of  $f_{82}$  been determined for IEPOX-  
146 SOA. Questions also have been raised about the uniqueness of this tracer and potential  
147 contributions from monoterpene SOA (Anonymous\_Referee, 2014).

148 In this study, the IEPOX-SOA results reported in various field campaigns are summarized  
149 and compared to predicted gas-phase IEPOX concentrations from a global model to help confirm  
150 the robustness of the AMS identification of this type of SOA. We then investigate the usefulness  
151 and limitations of the IEPOX-SOA tracers  $f_{C_5H_6O}$  ( $= C_5H_6O^+/OA$ ) and  $f_{82}$  by combining AMS  
152 data from multiple field and laboratory studies including a new dataset from the 2013 Southern  
153 Oxidant and Aerosol Study (SOAS). We compare the tracer levels in different OA sources  
154 (urban, biomass burning and biogenic), characterizing the background levels and interferences  
155 on this tracer for both high-resolution (HR) and unit mass resolution (UMR) data. We also

156 provide a simplified method to rapidly estimate IEPOX-SOA from  $f_{C_5H_6O}$  and  $f_{82}$ . While this  
157 method is no substitute for a detailed IEPOX-SOA identification via PMF, it is a simple method  
158 to estimate IEPOX-SOA concentrations (or its absence) in real-time from AMS or ACSM  
159 measurements or under conditions in real-time, or where PMF analysis is not possible or is  
160 difficult to perform.

## 161 **2 Experimental**

162 We classify the field datasets used in this study into three categories: (1) studies strongly  
163 influenced by urban and biomass-burning emissions: Los Angeles area, US and Beijing, China  
164 (urban); Changdao island, downwind of China and Barcelona area, Spain (urban downwind);  
165 flight data from biomass-burning plumes and continental areas (NW and western, US) in  
166 SEAC4RS and DC3 campaigns; and biomass burning lab emissions (FLAME-3 study). (2)  
167 Studies strongly influenced by isoprene emissions, including a SE US forest site (SOAS  
168 campaign); Two pristine forest site and one forest site partially impacted by urban plumes in the  
169 Amazon rain forest (Brazil). The latter site is classified in this category because (i) high isoprene  
170 concentrations (e.g. 3 ppb in average peaks in the afternoon) were observed during the study; (ii)  
171 the impact of biogenic SOA formed during 1000 km where the air travels over the pristine forest  
172 upwind of Manaus; (iii) PMF results indicate an important impact of IEPOX-SOA at this site (de  
173 Sá et al., 2015); (iv) PTRMS results indicate a substantial concentration of the isoprene  
174 hydroperoxyde formed by low-NO chemistry. Borneo rain forest in Malaysia; and flight data  
175 from SE US flights from aircraft campaign (SEAC4RS); (3) Studies strongly influenced by  
176 monoterpene emissions in a pine forest in the Rocky Mountains and a European boreal forest.  
177 Locations and additional detailed information about these studies can be found in Fig. 1 and  
178 Table 1.

179 With the exception of SOAS, all of the campaigns included in this analysis have been  
 180 previously described elsewhere (Table 1). The SOAS campaign took place in a forested area of  
 181 the SE US during June and July, 2013 (Fig. 1) and has several ground sites. The new dataset  
 182 introduced below was acquired at the SEARCH supersite, Centreville (CTR), AL (32.95° N,  
 183 87.13°W). Some results from a different SOAS site (Look Rock, TN) are also discussed later  
 184 (Budisulistiorini et al., 2015). Relatively high average isoprene and monoterpene concentrations  
 185 of  $3.3 \pm 2.4$  ppb and  $0.7 \pm 0.4$  ppb, respectively, were observed in SOAS-CTR by on-line GC/MS.  
 186 Measurements of non-refractory aerosol components of submicron particles ( $PM_{10}$ ) were made  
 187 using an Aerodyne high-resolution time-of-flight aerosol mass spectrometer (HR-ToF-AMS,  
 188 “AMS” hereafter) (DeCarlo et al., 2006). By applying positive matrix factorization (PMF) to the  
 189 time series of organic mass spectra (Ulbrich et al., 2009), we separated contributions from  
 190 IEPOX-SOA and other sources/components of OA. The AMS PMF results used here are very  
 191 consistent with those from a separate HR-ToF-AMS operated by another group at the same site  
 192 (Xu et al., 2014). The global gas-phase IEPOX concentrations in 2013 were modeled at a  
 193 resolution of 2 x 2.5 degrees as described in Nguyen et al. (2015). The gas-phase chemistry of  
 194 isoprene in GEOS-Chem is based on Paulot et al (2009a;2009b) as described by Mao et al.  
 195 (2013).

196 In the following discussion, we denote the IEPOX-SOA factor from PMF as “IEPOX-  
 197  $SOA_{PMF}$ ” and IEPOX-SOA from lab studies as “IEPOX- $SOA_{lab}$ ” for clarity. If we use “IEPOX-  
 198 SOA” in the paper, it refers to a broad concept of IEPOX-SOA. We use a superscript to clarify  
 199 the type of OA for which  $f_{C_5H_6O}$  is being discussed:  $f_{C_5H_6O}^{OA}$  refers to  $f_{C_5H_6O}$  in total OA,  
 200  $f_{C_5H_6O}^{IEPOX-SOA}$  to  $f_{C_5H_6O}$  in IEPOX- $SOA_{PMF}$  or IEPOX- $SOA_{lab}$ ,  $f_{C_5H_6O}^{MT-SOA}$  to the  $f_{C_5H_6O}$  value in pure  
 201 MT-SOA and  $f_{C_5H_6O}^{OA-Bkg-UB}$  and  $f_{C_5H_6O}^{OA-Bkg-MT}$  refer to background  $f_{C_5H_6O}^{OA}$  from areas strongly



202 influenced by urban+biomass-burning emissions and by monoterpene emissions, respectively. If  
203 we refer to  $f_{C_5H_6O}$  in general, we will still use  $f_{C_5H_6O}$ . When we report the average  $f_{C_5H_6O}^{OA}$  in each  
204 campaign, as shown in the Table 1, we used the average from the time series of  $f_{C_5H_6O}^{OA}$  at their  
205 raw time resolution (secs to mins). During this process, we exclude points whose OA mass  
206 concentrations are below twice the detection limit of OA in AMS (typically  $2 \times 0.26 \mu\text{g m}^{-3} = 0.5$   
207  $\mu\text{g m}^{-3}$ ). When averaging  $f_{C_5H_6O}^{OA}$  values across datasets, we counted each dataset as one data  
208 point.

### 209 **3 Results and Discussion**

#### 210 **3.1 IEPOX-SOA in a SE US forest during SOAS, 2013**

211 We use the SOAS-CTR field study (SE US-CTR) as an example for the determination of  
212 IEPOX-SOA from AMS data via PMF analysis. The time series and mass spectrum of this  
213 component are shown in Fig. 2. The IEPOX-SOA<sub>PMF</sub> mass concentration is the sum of mass  
214 concentrations of all the ions in the IEPOX-SOA<sub>PMF</sub> mass spectra. The “mass concentration” of  
215 an ion is used to represent the mass of the species whose detection resulted in the observed ion  
216 current of that ion, based on the properties of electron ionization (Jimenez et al., 2003). An  
217 uncertainty (standard deviation) of IEPOX-SOA<sub>PMF</sub> mass concentration of ~9% was estimated  
218 from 100 bootstrapping runs in PMF analysis (Ulbrich et al., 2009) (Fig. S1). This uncertainty  
219 concerns only the PMF separation method. In practice the uncertainty in IEPOX-SOA<sub>PMF</sub>  
220 concentration is dominated by the larger uncertainty on the AMS concentrations arising from the  
221 collection efficiency and relative ionization efficiency (Middlebrook et al., 2012).

222 A strong correlation is found between AMS IEPOX-SOA<sub>PMF</sub> and 2-methyltetrols ( $R=0.79$ )  
223 and sulfate ( $R = 0.75$ ) as expected (Surratt et al., 2010; Lin et al., 2012; Nguyen et al., 2014; Xu et

224 al., 2014). The diurnal variation of IEPOX-SOA<sub>PMF</sub> is also similar to gas-phase IEPOX and  
225 isoprene measured in SOAS-CTR. 2-Methyltetrols, measured on-line by GC-EI/MS with the SV-  
226 TAG instrument (Isaacman et al., 2014), comprise 26% of IEPOX-SOA<sub>PMF</sub> in SOAS-CTR on  
227 average, as shown in Fig. 2b. A similar ratio (29%) is found between 2-methyltetrols measured  
228 by offline analysis of filter samples using GC-EI/MS and LC/MS (Lin et al., 2014) and IEPOX-  
229 SOA<sub>PMF</sub>. Other IEPOX-SOA tracers, such as C5-alkene triols, IEPOX-organosulfates, and  
230 dimers containing them, can also be measured by offline GC-EI/MS and LC/MS (Lin et al.,  
231 2014; Budisulistiorini et al., 2015), and they account for 28% and 24% in total IEPOX-SOA<sub>PMF</sub>  
232 in SOAS (R=0.7), respectively (Fig. S2). The total IEPOX-SOA tracers measured in SOAS  
233 account for  $\sim 78 \pm 42\%$  of the total IEPOX-SOA<sub>PMF</sub> mass concentration. The uncertainty of the  
234 fraction of IEPOX-SOA molecular tracers in IEPOX-SOA<sub>PMF</sub> in SOAS study (42%) is estimated  
235 by combining the overall uncertainty from IEPOX-SOA molecular tracer measurement (24%),  
236 linear regression between tracer vs IEPOX-SOA<sub>PMF</sub> (17%, see Fig. 2b and Fig. S2), IEPOX-  
237 SOA<sub>PMF</sub> in PMF separation method (9%) and the quantification of IEPOX-SOA<sub>PMF</sub> based on  
238 AMS calibration (30%) (Middlebrook et al., 2012). This is a remarkably high value compared to  
239 the tracer to total SOA ratios for other SOA systems (e.g., SOA from monoterpenes or aromatic  
240 hydrocarbons) (Lewandowski et al., 2013). A total tracers to IEPOX-SOA<sub>PMF</sub> ratio of 26% was  
241 reported for the Look Rock site in SOAS (SOAS-LR) (Budisulistiorini et al., 2015). Thus, the  
242 measured total molecular tracer fraction in total IEPOX-SOA appears to be quite variable (a  
243 factor of 3) even if the same or similar techniques are used. Although the calibration  
244 methodology between different campaigns may result in some uncertainties, this value likely  
245 changes significantly between different times and locations, potentially due to changes in

246 particle-phase reaction conditions such as sulfate and water concentrations, acidity, and the  
247 identity and concentrations of oligomerization partners.

248 IEPOX-SOA<sub>PMF</sub> accounts for 17% of the total OA mass concentration at SOAS-CTR. This is  
249 shown in Fig. 1 along with the IEPOX-SOA<sub>PMF</sub> fraction from several previous studies (Robinson  
250 et al., 2011; Slowik et al., 2011; Budisulistiorini et al., 2013; Hayes et al., 2013; Hu et al.,  
251 2013; Chen et al., 2014; Hu et al., 2015). Fig. 1 also shows the surface gas-phase IEPOX  
252 concentrations for July, 2013 as simulated with GEOS-Chem. At all sites with at least ~30 ppt  
253 predicted average IEPOX concentration, IEPOX-SOA<sub>PMF</sub> is identified in AMS data. IEPOX-  
254 SOA<sub>PMF</sub> accounts for 6% – 36% of total OA in those studies, signifying the importance of  
255 IEPOX-SOA for regional and global OA budgets. No IEPOX-SOA<sub>PMF</sub> factor (i.e. below the  
256 PMF detection limit of ~5% of OA, Ulbrich et al., 2009) was found in areas strongly influenced  
257 by urban emissions where high NO concentrations suppress the IEPOX pathway, even in the  
258 presence of substantial isoprene concentrations (e.g. Hayes et al., 2013). GEOS-Chem indeed  
259 predicts negligible modeled gas-phase IEPOX concentrations in those areas, where isoprene  
260 peroxy radicals are expected to react primarily with NO. Some IEPOX can also be formed via  
261 high NO chemistry (Jacobs et al., 2014), however this pathway is thought to be much smaller  
262 than the low-NO pathway, consistent with the lack of observation of IEPOX-SOA<sub>PMF</sub> in the  
263 polluted studies included here. The fraction of IEPOX-SOA<sub>PMF</sub> positively correlates with  
264 modeled gas-phase IEPOX, as shown in the inset of Fig. 1.

265 The mass spectrum of IEPOX-SOA during SOAS-CTR is similar to those from other studies  
266 as seen in Fig. S3 – S4 (Robinson et al., 2011; Lin et al., 2012; Budisulistiorini et al., 2013; Chen  
267 et al., 2014; Nguyen et al., 2014; Xu et al., 2014), and also exhibits a prominent C<sub>5</sub>H<sub>6</sub>O<sup>+</sup> peak at  
268 *m/z* 82. We investigated the correlation between the time series of IEPOX-SOA<sub>PMF</sub> and each ion

269 in the OA spectra. The temporal variation of ion  $C_5H_6O^+$  correlates best ( $R=0.96$ ) with IEPOX-  
270  $SOA_{PMF}$  among all measured OA ions (Table S1). This result suggests that  $C_5H_6O^+$  ion may be  
271 the best ion tracer for IEPOX-SOA among all OA ions.  $C_5H_5O^+$  ( $m/z$  81),  $C_4H_5^+$  ( $m/z$  53),  
272  $C_4H_6O^+$  ( $m/z$  70) and  $C_3H_7O_2^+$  ( $m/z$  75) also correlate well with IEPOX- $SOA_{PMF}$  in SOAS-CTR  
273 and could be potential tracers for IEPOX- $SOA_{PMF}$ . Scatter plots between these four ions and  
274  $C_5H_6O^+$  at different campaigns indicate they either have higher background values or lower  
275 signal-to-noise compared to  $C_5H_6O^+$  (Fig. S5).

276  $f_{C_5H_6O}^{IEPOX-SOA}$  from SOAS and other field and laboratory studies (Table 1) ranges from 12‰ to  
277 40‰ (‰=parts per thousand) and have an average value of  $22\pm 7\%$ . The average  $f_{C_5H_6O}^{IEPOX-SOA}$   
278 value shown here also includes  $f_{82}$  data from four UMR IEPOX- $SOA_{PMF}$  spectra. This is justified  
279 since  $C_5H_6O^+$  accounts for over 95% of  $m/z$  82 in IEPOX-SOA based on results from SOAS-  
280 CTR and other lab studies (Kuwata et al., 2015). Indeed the average does not change if the UMR  
281 studies are removed from the average. These values are substantially higher than those from  
282 other types of OA or from locations with little impact from IEPOX-SOA, as discussed below.

### 283 **3.2 $f_{C_5H_6O}$ in areas with strong influence from urban and biomass burning emissions**

284 We next examine whether POA or SOA from field studies in areas strongly influenced by  
285 urban and biomass-burning emissions and without substantial predicted gas-phase IEPOX  
286 concentrations or IEPOX-SOA contributions can lead to enhanced  $f_{C_5H_6O}^{OA}$ . Figure 3a shows the  
287 distribution of  $f_{C_5H_6O}^{OA}$  in this category of studies peaks at  $1.7\pm 0.1\%$  (range 0.02 – 3.5‰). Data  
288 from continental air masses sampled from aircraft over the western and northwest US (where  
289 isoprene emissions are low) are shown in Fig. 3b and show a similar range as the polluted ground  
290 sites.

291 Biomass burning emissions and plumes sampled over multiple studies show a similar range  
292 to the pollution studies, with some slightly higher values. The peak of the distribution of  $f_{C_5H_6O}^{OA}$   
293 from fresh biomass-burning smoke across many different biomasses during the FLAME-3 study  
294 is 2.0%. During the SEAC4RS aircraft campaign, many biomass burning plumes were sampled,  
295 where OA concentrations varied over a wide range (several tens to more than one thousand  $\mu\text{g}$   
296  $\text{m}^{-3}$ ). The average  $f_{C_5H_6O}^{OA}$  across these biomass-burning plumes was 1.75% with low variability  
297 ( $\sim 20\%$ ), see Fig. S6.

298 We also explore whether other anthropogenic primary OA (POA) emission sources could  
299 elevate  $f_{C_5H_6O}$  above the observed background levels of  $\sim 1.7\%$ . Figure 3c shows  $f_{C_5H_6O}$  for POA  
300 spectra from vehicle exhaust, cooking, coal combustion, and multiple pure chemical standards  
301 (e.g., some alcohols; di- or poly acids) (Canagaratna et al., 2015). Almost all the values are  
302 below 2%, with exceptions for one type of cooking POA at 3%, the polyol xylitol (4.2%), and  
303 some acids (5-Oxoazelaic acid = 4.8%, Gamma ketopimelic acid = 5.2%, ketopimelic acid =  
304 6.5%, 3-Hydroxy-3-Methylglutaric acid = 11.8%, Adipic acid = 16.4%). All the tracers  
305 resulting in elevated  $f_{C_5H_6O}$  contain multiple hydroxyl groups, and may result in furan-like  
306 structures via facile dehydration reactions (Canagaratna et al., 2015). Xylitol has been proposed  
307 as a tracer of toluene SOA (Hu et al., 2008). It has a similar structure to 2-methyltetrols, with 5 -  
308 OH groups instead of 4. In the AMS, xylitol may form the methylfuran structure through  
309 dehydration reactions like 2-methyltetrols. However,  $f_{C_5H_6O}$  in other toluene SOA tracers in our  
310 dataset show background levels of  $f_{C_5H_6O}$  ( $< 2\%$ ). Given the small fraction of xylitol in toluene  
311 SOA (Hu et al., 2008), xylitol is unlikely to increase  $f_{C_5H_6O}$  in anthropogenic SOA, consistent  
312 with our results.

313 In summary, in the absence of strong impacts from biogenic SOA, the AMS high resolution  
314 ion  $C_5H_6O^+$  has a clear and stable background, spanning a small range (0.02 – 3.5‰) with an  
315 average values around  $1.7 \pm 0.1‰$  ( $f_{C_5H_6O}^{OA-Bkg-UB}$ ), about an order of magnitude lower than the  
316 average value ( $22 \pm 7‰$ ) of  $f_{C_5H_6O}^{IEPOX-SOA}$ .

### 317 **3.3 Enhancements of $f_{C_5H_6O}$ in areas strongly influenced by isoprene emissions**

318 GEOS-Chem predicts much higher surface gas-phase IEPOX concentrations over the SE US  
319 and Amazon rainforest than those in temperate urban areas (Fig. 1). This is expected from high  
320 isoprene concentrations (e.g. 3.3 ppb in SOAS-CTR and 4 ppb in the Amazon) under low  
321 average NO concentrations ( $\sim 0.1$  ppb) (Karl et al., 2009; Ebben et al., 2011). Probability  
322 distributions of  $f_{C_5H_6O}^{OA}$  during both campaigns are shown in Fig. 4a, and are very similar with  
323 averages of 5 – 6‰ (range 2.5‰ – 11‰). The Amazon forest downwind of Manaus and a  
324 Borneo tropical forest study show even higher averages of 7‰ and 10‰, respectively (Robinson  
325 et al., 2011; de Sá et al., 2015). During the SEAC4RS aircraft campaign, the average  $f_{C_5H_6O}^{OA}$   
326 ( $4.4 \pm 1.6‰$ ) from all SE US flights is also enhanced compared to levels observed in the  
327 northwest and western US continental air masses ( $1.7 \pm 0.3‰$ ) where isoprene emissions are  
328 much smaller (Guenther et al., 2012). Thus, campaigns in locations strongly influenced by  
329 isoprene emissions under lower NO conditions show systematically higher  $f_{C_5H_6O}^{OA}$  values (with  
330 an average peak of  $6.5‰ \pm 2.2‰$ ) than background levels found in other locations (1.7‰). The  
331 fact that  $f_{C_5H_6O}^{OA}$  ( $6.5 \pm 2.2‰$ ) in these studies is lower than the values in IEPOX-SOA ( $22‰ \pm 7‰$ )  
332 is expected, since ambient datasets also include OA from other sources, and confirms that  
333 IEPOX-SOA is not an overwhelmingly dominant OA source at most of those locations (See Fig.  
334 S7).

### 3.4 Values of $f_{C_5H_6O}$ in laboratory studies of non IEPOX-derived isoprene SOA

We also investigate  $f_{C_5H_6O}$  in laboratory SOA from isoprene in Fig. 4a. For SOA produced by chamber isoprene photooxidation under high  $NO_x$  conditions, low  $f_{C_5H_6O}$  ( $<2\text{‰}$ ) within the background level is observed (Kroll et al., 2006; Chen et al., 2011). SOA from oxidation of isoprene hydroxyhydroperoxide (ISOPOOH, a product of low-NO oxidation of isoprene) under low-NO conditions, when formed under conditions that are not favorable for the reactive uptake of IEPOX into aerosols also has low  $f_{C_5H_6O}$  of 2‰ (Krechmer et al., 2015). Low values of  $f_{C_5H_6O}$  ( $<3\text{‰}$ ) are also observed in SOA from isoprene +  $NO_3$  radical reactions without acid seeds (Ng et al., 2008). The low  $f_{C_5H_6O}$  ( $<3\text{‰}$ ) observed in non IEPOX-derived isoprene SOA indicate that  $f_{C_5H_6O}$  is specifically enhanced from IEPOX-SOA, and is not a tracer for all SOA from isoprene.

### 3.5 Enhancements of $f_{C_5H_6O}$ in areas strongly influenced by monoterpene emissions

The BEACHON-RoMBAS campaign was carried out in a Rocky Mountain pine forest with high monoterpene emissions that account for 34% in daytime and 66 % at night of the total VOC mixing ratios (on average peaking at 0.15 ppb during day and 0.7 ppb at night) (Fry et al., 2013) but lower isoprene emissions (peaking at 0.35 ppb during daytime) (Kaser et al., 2013; Karl et al., 2014). One-third of the  $RO_2$  radicals react via the low-NO route (i.e. via  $RO_2 + HO_2$ ) at this site (Fry et al., 2013). The isoprene/monoterpene ratio at the Rocky Mountain site is 0.48, and is ~ 10 – 20 times lower than the value (4.7) in SOAS-CTR and (8.3) in Amazon studies (Chen et al., 2014), suggesting that  $f_{C_5H_6O}^{OA}$  may be near background levels because of the very low potential contribution of IEPOX-SOA at the Rocky Mountain site. However, the average  $f_{C_5H_6O}^{OA}$  at the Rocky Mountain site is  $3.7 \pm 0.5\text{‰}$  (Fig. 4a), which although lower than the average  $f_{C_5H_6O}^{OA}$

357 (6.5‰) found in the SE US-CTR, Amazon and Borneo forests, it is still twice the

358  $f_{C_5H_6O}^{OA-Bkg-UB}$  values of 1.7‰ observed in pollution and smoke-dominated locations.

359 Three circumstances may lead to such an enhanced  $f_{C_5H_6O}^{OA}$  at the Rocky Mountain site, which  
360 we examine here. (1) A small amount of IEPOX-SOA may be formed from the limited isoprene  
361 present at the Rocky Mountain site and surrounding region. However, the average isoprene  
362 concentration in this pine forest area is only 0.2 ppb, which is around 16 times less than that (3.3  
363 ppb) at the SE US site in SOAS. The conditions at the Rocky Mountain site were less favorable  
364 for IEPOX-SOA formation due to a higher fraction (70% in daytime) of the RO<sub>2</sub> radicals  
365 reacting with NO and less acidic aerosols (Fry et al., 2013;Levin et al., 2014). Thus we can  
366 estimate an upper limit contribution of IEPOX-SOA to the  $f_{C_5H_6O}^{OA}$  tracer at the Rocky Mountain  
367 site assuming the same ratio of IEPOX-SOA to isoprene in both campaigns. In this case, we  
368 would expect  $f_{C_5H_6O}^{OA}$  at the Rocky Mountain site to be the background level (1.7‰) plus 1/16<sup>th</sup> of  
369 the enhancement above the background observed in SOAS (5‰ – 1.7‰ = 3.3‰) multiplied by  
370 the ratio of OA concentrations at both sites (4.8 µg m<sup>-3</sup> in SE US site vs 1.8 µg m<sup>-3</sup> in Rocky  
371 Mountain site). This calculation results in an expected upper limit  $f_{C_5H_6O}^{OA} \sim 2.25‰$  at the Rocky  
372 Mountain site due to the IEPOX-SOA contribution. This estimate is much lower than the  
373 observed average 3.7‰. Thus the elevated  $f_{C_5H_6O}^{OA}$  in Rocky Mountain pine forest is very unlikely  
374 to be due to IEPOX-SOA.

375 (2) The second explanation of high  $f_{C_5H_6O}^{OA}$  observed at Rocky Mountain site is that SOA from  
376 monoterpene oxidation (MT-SOA) may have a higher  $f_{C_5H_6O}$  than background OA from other  
377 sources. Several chamber studies show that MT-SOA, e.g., SOA from ozonolysis (Chhabra et al.,  
378 2011;Chen et al., 2014) or photooxidation (Ng et al., 2007) of  $\alpha$ -pinene, or NO<sub>3</sub> reaction with  $\alpha$ -  
379 pinene, or NO<sub>3</sub> reaction with  $\alpha$ -pinene,  $\beta$ -pinene and  $\Delta^3$ -Carene (Fry et al., 2014;Boyd et al.,



380 2015) can result in higher  $f_{C_5H_6O}$  (average  $5.5 \pm 2.0\%$ ) than background levels of  $\sim 1.7\%$  (Fig. 4a).  
381 We note that the average lab-generated MT-SOA value ( $f_{C_5H_6O}^{MT-SOA}$ ) is still 4 times lower than the  
382 average  $f_{C_5H_6O}^{IEPOX-SOA}$  for IEPOX-SOA<sub>PMF</sub> and IEPOX-SOA<sub>lab</sub> (Fig. S8), and thus there is some  
383 room to separate both contributions. Oxidation of monoterpenes can lead to species with multiple  
384 –OH groups, which may result in the production of methylfuran (or ions of similar structure)  
385 upon AMS analysis. We do not observe enhanced  $f_{C_5H_6O}$  in SOA from sesquiterpene oxidation  
386 ( $< 2\%$ ) (Chen et al., 2014). The values of  $f_{C_5H_6O}^{MT-SOA}$  in chamber studies, together with the finding  
387 of a substantial contribution of monoterpenes to SOA at this Rocky Mountain site (Fry et al.,  
388 2013) suggest that MT-SOA may explain the values of  $f_{C_5H_6O}^{OA}$  observed there.

389 Two other field studies support the conclusion that ambient MT-SOA may have slightly  
390 enhanced  $f_{C_5H_6O}$ . Fig. 6 shows data from a DC3 aircraft flight in the areas around Missouri and  
391 Illinois. Ambient  $f_{C_5H_6O}^{OA}$  increases from background levels ( $\sim 1.7\%$ ) to  $\sim 4.1\%$  in a highly  
392 correlated manner to monoterpene concentration increases (with an average of  $3.0\%$  during the  
393 enhanced period). Meanwhile, isoprene and gas-phase IEPOX stay at low levels similar to the  
394 rest of the flight, indicating that enhanced  $f_{C_5H_6O}^{OA}$  in the periods with higher MT concentrations  
395 should arise from MT-SOA and not IEPOX-SOA. Fig. 4a includes AMS measurements at a MT-  
396 emission dominated European boreal forest (Hyytiälä in Finland) (Robinson et al., 2011).  
397 Average  $f_{C_5H_6O}^{OA}$  is  $\sim 2.5\%$  at this site, which is again higher than the  $f_{C_5H_6O}^{OA-Bkg-UB}$  value of  $1.7\%$ .  
398 The slightly lower  $f_{C_5H_6O}^{OA}$  in the Boreal forest vs. the Rocky Mountain site may be partially  
399 explained by a small contribution from IEPOX-SOA at the latter (estimated above to increase  
400  $f_{C_5H_6O}^{OA}$  up to  $2.25\%$  at the Rocky Mountain site), as well as by differences of the MT-SOA/OA

401 ratio at both sites (Corrigan et al., 2013) and the relative importance of different MT species and  
402 oxidation pathways.

403 (3) The enhanced  $f_{C_5H_6O}^{OA}$  at the Rocky Mountain site may have arisen from oxidation  
404 products of 2-methyl-3-buten-2-ol (MBO,  $C_5H_{10}O$ ) emitted from pine trees. MBO, with a  
405 daytime average of 2 ppb accounts for ~50% of the total VOC mixing ratio during the day (Karl  
406 et al., 2014). MBO has been shown to form aerosol with a 2 – 7 % yield in chamber studies,  
407 which is thought to proceed via the uptake of epoxide intermediates ( $C_5H_{10}O_2$ , vs. IEPOX  
408  $C_5H_{10}O_3$ ) under acidic aerosol conditions (Zhang et al., 2012; Mael et al., 2014; Zhang et al.,  
409 2014). Some aerosol species formed by MBO-derived epoxides have similar structures (e.g.,  
410  $C_5H_{12}O_3$ ) to the IEPOX oxidation products in SOA and thus they might contribute to  $f_{C_5H_6O}^{OA}$ . No  
411 pure MBO-derived epoxides or their oxidation products in the aerosol phase have been measured  
412 by AMS so far, to our knowledge.

413 To attempt to differentiate whether MT-SOA or MBO-SOA dominate the higher  $f_{C_5H_6O}^{OA}$  at  
414 the Rocky Mountain site, average diurnal variations of ambient  $f_{C_5H_6O}^{OA}$ , monoterpene and  
415 isoprene+MBO are plotted in Fig. S9.  $f_{C_5H_6O}^{OA}$  shows a diurnal pattern that increases at night and  
416 peaks in the early morning, similar to the diurnal variation of monoterpenes. Monoterpenes  
417 continue to be oxidized during nighttime at this site by  $NO_3$  radical and  $O_3$  with a lifetime of ~30  
418 min (with 5 ppt of  $NO_3$  and 30 ppb of  $O_3$ ) (Fry et al., 2013). In contrast only a decrease and later  
419 a plateau of  $f_{C_5H_6O}^{OA}$  are observed during the period with high MBO concentration and higher  
420 oxidation rate of MBO due to high OH radical in daytime (as MBO reacts slowly with  $O_3$  and  
421  $NO_3$ ) (Atkinson and Arey, 2003). While MBO-SOA may or may not have  $f_{C_5H_6O}^{OA}$  above  
422 background levels, the diurnal variations point to MT-SOA playing a dominant role in  $f_{C_5H_6O}^{OA}$  at  
423 this site.

424 The average  $f_{C_5H_6O}^{OA}$  in areas strongly influenced by monoterpene emissions is  $3.1\pm 0.6\%$ ,  
425 obtained by averaging the values from the Rocky mountain forest (3.7‰), European boreal  
426 forest (2.5‰), and DC3 flight (3.0‰). Note that the difference between  $f_{C_5H_6O}^{OA}$  in areas strongly  
427 influenced by monoterpene emissions ( $3.1\pm 0.6\%$ ) and isoprene emissions ( $6.5\pm 2.2\%$ ) is  
428 reduced, compared to a factor of 4 differences between pure MT-SOA ( $5.5\pm 2.0\%$ ) and IEPOX-  
429 SOA ( $22\pm 7\%$ ). This is likely due to the physical mixing of OA from different sources and in  
430 different proportions at each location.

### 431 **3.6 $f_{C_5H_6O}$ vs OA oxidation level ( $f_{CO_2}$ ) “triangle plot” – background studies**

432 In AMS spectra, the  $CO_2^+$  ion is a marker of aging and oxidation processes (Alfarra et al.,  
433 2004; Ng et al., 2011a). To evaluate whether oxidation plays a role on the observed  $f_{C_5H_6O}$  for  
434 different types of OA, in this section we use plots of  $f_{CO_2}$  (=  $CO_2^+/OA$ ) vs.  $f_{C_5H_6O}$  as a graphical  
435 diagnostic of this process, similar to graphical diagnostics (“triangle plots”) used for other  
436 purposes with AMS data (Cubison et al., 2011; Ng et al., 2011a). For studies strongly influenced  
437 by urban and biomass-burning emissions in Fig. 3d we observe a wide range of  $f_{CO_2}^{OA}$  values from  
438 0.001 to 0.3 (= 30% or 300‰). The wide range of  $f_{CO_2}^{OA}$  is due to variable fractions of POA and  
439 SOA (mixing effect) and a variable oxidation level of POA and SOA (oxidation effect) in the  
440 different studies. In fact, to our knowledge, these studies encompass the values of  $f_{CO_2}^{OA}$  observed  
441 in all ambient AMS studies to date (Ng et al., 2011a). Several studies when urban and forest air,  
442 or biomass burning smoke were aged by intense OH oxidation with an oxidation flow reactor  
443 (OFR) (Kang et al., 2007; Li et al., 2013; Ortega et al., 2013) are also included. However, despite  
444 the wide range of  $f_{CO_2}^{OA}$ ,  $f_{C_5H_6O}^{OA}$  changes little, staying in the range 0.02 – 3.5‰, and with little  
445 apparent dependence on  $f_{CO_2}^{OA}$  for the ambient studies. A linear regression to quantiles from this

446 dataset results in an intercept of 1.7‰ and a very weak decrease with increasing  $f_{CO_2}^{OA}$ . A stronger  
447 decrease is observed when aging urban air (Los Angeles) by intense OH exposure in flow  
448 reactor, as shown in Fig. 3d.

449 Ambient  $f_{CO_2}^{OA}$  at the Rocky Mountain forest site shows a moderate oxidation level (0.1 –  
450 0.15), similar to the SE US-CTR (Fig. 5).  $f_{C_5H_6O}^{OA}$  in the Rocky mountain site decreases linearly  
451 when  $f_{CO_2}^{OA}$  increases. During the Rocky Mountain study, the intense OH aging of ambient air in a  
452 flow reactor shows a continuation of the trend observed for the ambient data, where  $f_{C_5H_6O}^{OA}$   
453 decreases as  $f_{CO_2}^{OA}$  increases. A linear regression to the combined ambient and OFR datasets  
454 ( $f_{C_5H_6O}^{OA} = -0.013 \times f_{CO_2}^{OA} + 0.0054$ ) will be used below to estimate background  $f_{C_5H_6O}^{OA}$  in areas with  
455 strong monoterpene and low isoprene emissions.

456  $f_{C_5H_6O}$  in ambient SOA from other studies catalogued in the HR-AMS spectral database are  
457 also shown in Fig. 5. Most urban oxygenated OA (OOA) are within  $f_{C_5H_6O}^{OA-Bkg-UB}$  (average 1.7‰;  
458 range: 0.02 – 3.5‰), which is consistent with the  $f_{C_5H_6O}$  (<3‰) in lab aromatic SOA and other  
459 urban OA in Fig. 5. However, some ambient SOA spectra do show higher  $f_{C_5H_6O}$  (3 – 10‰) than  
460 the  $f_{C_5H_6O}^{OA-Bkg-UB}$  (0.02 – 3.5‰), which we will discuss in the next section.

### 461 **3.7 $f_{C_5H_6O}$ vs. OA oxidation level ( $f_{CO_2}$ ) – IEPOX-SOA influenced Studies**

462  $f_{CO_2}^{OA}$  vs.  $f_{C_5H_6O}^{OA}$  in studies impacted by IEPOX-SOA are shown in Fig. 5. Consistent with the  
463 distributions discussed above, the bulk of points from these areas all show distinctively enhanced  
464  $f_{C_5H_6O}^{OA}$  when compared to background  $f_{C_5H_6O}^{OA}$  points of similarly moderate or higher oxidation  
465 levels. The  $f_{C_5H_6O}^{OA}$  measurements with lower  $f_{CO_2}^{OA}$  values are more broadly distributed than the  
466  $f_{C_5H_6O}^{OA}$  points with higher  $f_{CO_2}^{OA}$  values in SE US-CTR, SEAC4RS, Borneo forest and Amazon

467 forest downwind of Manaus. However, increased  $f_{C_5H_6O}^{OA}$  with higher  $f_{CO_2}^{OA}$  was observed in the  
468 Amazon. Both oxidation and mixing of airmasses with different OA can influence these  
469 observations.  $f_{C_5H_6O}^{IEPOX-SOA}$  in IEPOX-SOA usually will decrease with oxidative aging. E.g.,  
470  $f_{C_5H_6O}^{OA}$  from the SOAS oxidation flow reactor decreases continuously as OA becomes more  
471 oxidized than ambient OA in SOAS-CTR ( $f_{CO_2}^{OA}$  increases from 0.15 to 0.3). Airmass mixing  
472 effects are more complex. Depending on the  $f_{CO_2}^{OA}$  in the airmasses mixed with,  $f_{C_5H_6O}^{OA}$  in IEPOX-  
473 SOA-rich air can show positive, neutral or negative trends with increasing  $f_{CO_2}^{OA}$ . E.g., in pristine  
474 Amazon forest, points with both lower  $f_{CO_2}^{OA}$  (<0.08) and  $f_{C_5H_6O}^{OA}$  (< 8‰) values are thought to be  
475 mainly caused by advection of POA from occasional local pollution.

476 The overall trend for the ambient measurements in studies strongly influenced by isoprene  
477 emissions (Fig. 5) is that those points cluster in a triangle shape and  $f_{C_5H_6O}^{OA}$  decreases as  $f_{CO_2}^{OA}$   
478 increases, as illustrated in Fig. S10. This “triangle shape” indicates that as the ambient OA  
479 oxidation increases, the IEPOX-SOA signature is reduced, potentially by the ambient oxidation  
480 processes or by physical mixing with airmasses containing more aged aerosols.

481 Finally, points with higher  $f_{C_5H_6O}$  in OOA/aged OA are labeled with numbers in Fig. 5. The  
482 sources of those labeled points are summarized in Table S2. OA from those studies are all  
483 partially influenced by biogenic emissions. For example, during measurements of ambient OA in  
484 the Central Valley of California (number 2), high isoprene emissions and acidic particles were  
485 observed (Dunlea et al., 2009), suggesting that potential IEPOX-SOA formed in this area may  
486 explain the higher  $f_{C_5H_6O}^{OA}$  there.

### 487 **3.8 Best estimate of $f_{C_5H_6O}$ in IEPOX-SOA**

488 IEPOX-SOA from different field campaigns and chamber studies lay towards the right and  
489 on the bottom half of Fig. 5. IEPOX-SOA from chamber studies show systematically lower  
490  $f_{CO_2}^{IEPOX-SOA}$  than ambient studies. This is likely explained by the lack of additional aging in the  
491 laboratory studies, because all the lab IEPOX-SOA were measured directly after uptake gas-  
492 phase IEPOX onto acidic aerosol without undergoing substantial additional oxidation.

493 A wide range (12 – 40‰) of  $f_{C_5H_6O}^{IEPOX-SOA}$  is observed with an average of  $22‰ \pm 7‰$  in  
494 ambient and lab IEPOX-SOA.  $f_{C_5H_6O}^{IEPOX-SOA}$  did not show a trend vs.  $f_{CO_2}^{IEPOX-SOA}$ . The IEPOX-  
495 SOA molecular tracer 3-MeTHF-3,4-diols has been shown to enhance the  $f_{C_5H_6O}$  in OA (Fig. 5)  
496 (Lin et al., 2012; Canagaratna et al., 2015). Except 3-MeTHF-3,4-diols none of the other pure  
497 IEPOX-derived polyols standards have been atomized and injected into the AMS system so far,  
498 to our knowledge. We suspect other polyols such as 2-methyltetrols may also lead to such an  
499 enhancement through dehydration reactions in the AMS vaporizer leading to methylfuran-type  
500 structures. The diversity of  $f_{C_5H_6O}^{IEPOX-SOA}$  in different studies is related with the variable content of  
501 specific IEPOX-SOA molecular species that enhance  $f_{C_5H_6O}^{IEPOX-SOA}$  differently. The fractions of  
502 molecular IEPOX-SOA species in total IEPOX-SOA<sub>PMF</sub> is plotted vs  $f_{C_5H_6O}^{IEPOX-SOA}$  in three  
503 different studies in Fig. 7, which show a strong correlation between each other. The strong  
504 simultaneous variation of both quantities indicates that the diversity of  $f_{C_5H_6O}^{IEPOX-SOA}$  is very likely  
505 explained by the variability of the molecules comprising IEPOX-SOA among different studies.

506 During one day in SOAS (June 26<sup>th</sup>, 2013), IEPOX-SOA<sub>PMF</sub> comprised 80 – 90% of total  
507 OA (Fig. S11), possibly due to high sulfate concentrations favoring IEPOX-SOA formation.  
508  $f_{C_5H_6O}^{OA}$  reached 25‰, which is similar to the 22‰ for the IEPOX-SOA<sub>PMF</sub> from this study, and  
509 consistent with a slightly lower value for the average vs. freshest ambient IEPOX-SOA. Among  
510 the chamber studies, the study of reactive uptake of isoprene-oxidation products into an acidic

511 seed is most similar to the full chemistry in real ambient environments (Liu et al., 2014), and  
 512 reports similar  $f_{C_5H_6O}^{IEPOX-SOA}$  values (19%). Hence, we propose an average  $f_{C_5H_6O}^{IEPOX-SOA}$  (22%)  
 513 from both studies as the typical value of fresh IEPOX-SOA.

### 514 3.9 Proposed Method for Real-Time Estimation of IEPOX-SOA

515 So far, PMF of AMS spectra is the only demonstrated method for quantifying total IEPOX-  
 516 SOA concentrations. However, the PMF method is labor-intensive and requires significant  
 517 expertise, and may fail to resolve a certain factor when present in lower mass fractions (<5%). A  
 518 simpler, real-time method to estimate IEPOX-SOA would be useful in many studies, including  
 519 ground-based and aircraft campaigns.

520 We propose an estimation method for IEPOX-SOA based on the mass concentration of its  
 521 tracer ion  $C_5H_6O^+$ . To do this, we express the mass concentration of  $C_5H_6O^+$  as

$$522 \quad C_5H_6O_{total}^+ = C_5H_6O_{IEPOX-SOA,ambient}^+ + C_5H_6O_{background}^+. \quad (1)$$

523 Where,  $C_5H_6O_{total}^+$  is measured total  $C_5H_6O^+$  signal in AMS;  $C_5H_6O_{IEPOX-SOA,ambient}$  and  
 524  $C_5H_6O_{background}^+$  are the  $C_5H_6O^+$  signals contributed by IEPOX-SOA in ambient OA and other  
 525 background OA (non IEPOX-SOA).

526 Then,  $C_5H_6O_{IEPOX-SOA,ambient}$  and  $C_5H_6O_{background}^+$  can be calculated as:

$$527 \quad C_5H_6O_{IEPOX-SOA,ambient}^+ = IEPOX-SOA \times f_{C_5H_6O}^{IEPOX-OA}. \quad (2)$$

$$528 \quad C_5H_6O_{background}^+ = (OA_{mass} - IEPOX-SOA) \times f_{C_5H_6O}^{OA-Bkg}. \quad (3)$$

529 Where,  $f_{C_5H_6O}^{IEPOX-OA}$  is the fractional contribution of  $C_5H_6O^+$  to the total ion signal in the  
 530 spectra of IEPOX-SOA from  $IEPOX-SOA_{lab}$  or  $IEPOX-SOA_{PMF}$  factors.  $f_{C_5H_6O}^{OA-Bkg}$  is the  
 531 background  $f_{C_5H_6O}$  in other non-IEPOX-SOA, e.g., values from OA strongly influenced by urban  
 532 and biomass-burning emissions ( $f_{C_5H_6O}^{OA-Bkg-UB}$ ).

533 Then, by combining Eq. (1) – (3), we can express  $C_5H_6O^+_{total}$  as:

534 
$$C_5H_6O^+_{total} = IEPOX-SOA \times f_{C_5H_6O}^{IEPOX-OA} + (OA - IEPOX-SOA) \times f_{C_5H_6O}^{OA-Bkg}. \quad (4)$$

535 Finally, IEPOX-SOA can be estimated as:

536 
$$IEPOX-SOA = \frac{C_5H_6O^+_{total} - OA \times f_{C_5H_6O}^{OA-Bkg}}{f_{C_5H_6O}^{IEPOX-OA} - f_{C_5H_6O}^{OA-Bkg}}. \quad (5)$$

537 In Eq. (5),  $C_5H_6O^+_{total}$  and OA mass are measured directly by AMS.  $f_{C_5H_6O}^{OA-Bkg}$  and

538  $f_{C_5H_6O}^{IEPOX-OA}$  are two parameters that must be determined by other means.

539 As discussed above, the background value in the absence of a substantial impact of MT-

540 SOA is  $\sim 1.7\%$ . In studies influenced by monoterpene emissions, the background value may be

541 elevated by MT-SOA.  $f_{C_5H_6O}^{OA}$  at the Rocky Mountain site estimated by  $f_{C_5H_6O}^{OA} = (0.41 -$

542  $f_{CO_2}^{OA}) \times 0.013$  (Fig. 5) can be used as  $f_{C_5H_6O}^{OA-Bkg}$  for areas with strong MT-SOA contributions

543 ( $f_{C_5H_6O}^{OA-Bkg-MT}$ ). There is some uncertainty in this value, due to possible contributions of a small

544 amount of IEPOX-SOA, MBO-SOA, and other OA sources at this site. An alternative estimate

545 for  $f_{C_5H_6O}^{OA-Bkg-MT}$  would be  $\sim 1.7\% + 3 \times MT_{avg}$  (ppb), which is also approximately consistent with

546 our ambient data, but may have higher uncertainty. Further characterization of the background

547  $f_{C_5H_6O}$  in areas with MT-SOA impact is of interest for future studies. Finally, we have decided to

548 use  $f_{C_5H_6O}^{OA}$  estimated from the Rocky Mountain site as  $f_{C_5H_6O}^{OA-Bkg-MT}$  in the following calculation.

549 As discussed above, we use average  $f_{C_5H_6O}^{IEPOX-OA} = 22\%$  in Eq. (3) as a representative value of

550 ambient IEPOX-SOA. Several scenarios based on different  $f_{C_5H_6O}^{OA}$  values to use this tracer-based

551 method are addressed in the supporting information. The justification from users on using this

552 method is needed.



### 553 3.10 Application of the Real-Time Estimation Method of IEPOX-SOA

554 To test the proposed estimation method, we use SE US forest (SOAS) data as an example in  
555 Fig. 8, applying both background estimates (urban & biomass burning, and monoterpene  
556 emissions). Since there are high monoterpene concentrations (~1 ppb during the night) in SOAS,  
557 we expect the MT-influenced background to be more accurate. The IEPOX-SOA estimated by  
558 subtracting the MT-SOA background (IEPOX-SOA<sub>MT</sub>) is indeed better correlated with IEPOX-  
559 SOA<sub>PMF</sub> (R=0.99) than that (R = 0.96) when the urban & biomass-burning background is applied  
560 (IEPOX-SOA<sub>urb&bb</sub>). The intercept of regression line between IEPOX-SOA<sub>MT</sub> and IEPOX-  
561 SOA<sub>PMF</sub> is zero, indicating the background of IEPOX-SOA contributed by MT-SOA is clearly  
562 deducted.

563 The regression slope between IEPOX-SOA<sub>MT</sub> and IEPOX-SOA<sub>PMF</sub> is 0.95, suggesting that  
564 C<sub>5</sub>H<sub>6</sub>O<sup>+</sup> in SE US CTR site (SOAS) may be slightly overcorrected by minimizing C<sub>5</sub>H<sub>6</sub>O<sup>+</sup> from  
565 monoterpene emissions. This underestimation may be associated with higher MT-SOA  
566 contribution to C<sub>5</sub>H<sub>6</sub>O<sup>+</sup> in Rocky Mountain pine forest site than SE US forest site, or interference  
567 from IEPOX-SOA/MBO-SOA at the Rocky Mountain site. IEPOX-SOA<sub>urb&bb</sub> is 1.26 times  
568 higher than IEPOX-SOA<sub>PMF</sub>. Thus, as expected IEPOX-SOA<sub>MT</sub> and IEPOX-SOA<sub>urb&bb</sub> provide  
569 lower and upper limits of estimated IEPOX-SOA.

570 Among all the datasets introduced in this study, the SOAS-CTR dataset should be the best  
571 case scenario since  $f_{C_5H_6O}^{IEPOX-OA} = 22\%$  is coincidentally the same value in the spectrum of IEPOX-  
572 SOA<sub>PMF</sub> in SOAS-CTR and a large fraction (17%) of IEPOX-SOA existed in SOAS-CTR as  
573 well. Given the spread of values of  $f_{C_5H_6O}^{IEPOX-OA}$  (12 – 40%) in different studies, if no additional  
574 local IEPOX-SOA spectrum is available for a given site, the estimation from this method should

575 be within a factor of ~2 of the actual concentration, as illustrated in Fig. S13-S14. Further  
576 information concerning the estimation method using unit mass resolution  $m/z$  82 (or  $f_{82}$ ) can be  
577 found in the Appendix.

#### 578 4. Conclusions

579 To investigate if the ion  $C_5H_6O^+$  (at  $m/z$  82) in AMS spectra is a good tracer for IEPOX-SOA,  
580 tens of field and lab studies are combined and compared, including the SOAS 2013 campaign in  
581 the SE US. The results show that  $f_{C_5H_6O}^{OA}$  is clearly elevated when IEPOX-SOA is present, and  
582 thus has potential usefulness as a tracer of this aerosol type. The average  $f_{C_5H_6O}^{IEPOX-OA}$  in  
583 chamber and ambient studies is  $22 \pm 7\%$  (range 12% – 40%). No dependence of  $f_{C_5H_6O}^{IEPOX-OA}$  on  
584 oxidation level ( $f_{CO_2}^{IEPOX-SOA}$ ) was found. Background  $f_{C_5H_6O}$  in OA strongly influenced by urban  
585 or biomass-burning emissions or pure anthropogenic POAs averages  $1.7 \pm 0.1\%$  (range 0.02 –  
586 3.5%).

587 In ambient OA that is strongly influenced by isoprene emissions under lower NO, we observe  
588 systematically higher  $f_{C_5H_6O}^{OA}$  (with an average of  $\sim 6.5 \pm 2.2\%$ ), consistent with presence of  
589 IEPOX-SOA. Low tracer values ( $f_{C_5H_6O} < 3\%$ ) are observed in non IEPOX-derived isoprene-  
590 SOA from laboratory studies, indicating that the tracer ion is specifically enhanced from IEPOX-  
591 SOA, and is not a tracer for all SOA from isoprene.

592 Higher background values of  $f_{C_5H_6O}^{OA}$  ( $3.1 \pm 0.6\%$  in average) were found in area strongly  
593 impacted by monoterpene emissions.  $f_{CO_2}^{MT-SOA}$  is  $5.5 \pm 2.0\%$ , which are substantially lower than  
594 for IEPOX-SOA ( $22 \pm 7\%$ ), and thus they leave some room to separate both contributions. A

595  $f_{C_5H_6O}^{OA-Bkg-MT}$  as a function of  $f_{CO_2}^{OA}$  in monoterpene emissions is determined by linear regressing  
596 the  $f_{C_5H_6O}^{OA}$  and  $f_{CO_2}^{OA}$  at a Rocky Mountain pine forest site.

597 A simplified method to estimate IEPOX-SOA based on measured ambient  $C_5H_6O^+$ ,  $CO_2^+$  and  
598 OA in AMS is proposed. Good correlations ( $R>0.96$ ) between estimated IEPOX-SOA and  
599 IEPOX-SOA<sub>PMF</sub> are obtained for SOAS, confirming the potential usefulness of this estimation  
600 method. Given the observed variability in IEPOX-SOA composition, the method is expected to  
601 be within a factor of  $\sim 2$  of the true concentration if no additional information about the local  
602 IEPOX-SOA is available for a given study. When only unit mass resolution data is available as  
603 in ACSM data, all methods may perform less well because of increased interferences from other  
604 ions at  $m/z$  82.

605

606 **ACKNOWLEDGMENT**

607 This study was partially supported by NSF AGS-1243354 and AGS-1360834, NASA  
608 NNX12AC03G, DOE (BER/ASR) DE-SC0011105, and NOAA NA13OAR4310063. B. Palm  
609 and J. Krechmer are grateful for fellowships from EPA STAR (FP-91761701-0 and FP-  
610 91770901-0) and CIRES. A. Ortega is grateful for a CU-Boulder Chancellor's and DOE SCGF  
611 (ORAU/ORISE) fellowship. A. Wisthaler and T. Mikoviny were supported by the Austrian  
612 Federal Ministry for Transport, Innovation and Technology (BMVIT) through the Austrian  
613 Space Applications Programme (ASAP) of the Austrian Research Promotion Agency (FFG), and  
614 the Visiting Scientist Program at the National Institute of Aerospace (NIA). G. Isaacman-  
615 VanWertz is grateful for an NSF Fellowship (DGE-1106400). UC Berkeley was supported by  
616 NSF AGS-1250569. We acknowledge the logistical support from the LBA Central Office at INPA  
617 (Instituto Nacional de Pesquisas da Amazonia). P. Artaxo acknowledges support from FAPESP  
618 grants 2013/05014-0 and 2014/05238-8 and CNPq support from grants 457843/2013-6 and  
619 307160/2014-9. We acknowledge this work was funded by the U.S. Environmental Protection  
620 Agency (EPA) through grant number 835404. The contents of this publication are solely the  
621 responsibility of the authors and do not necessarily represent the official views of the U.S. EPA.  
622 Further, the U.S. EPA does not endorse the purchase of any commercial products or services  
623 mentioned in the publication. The U.S. EPA through its Office of Research and Development  
624 collaborated in the research described here. It has been subjected to Agency review and approved  
625 for publication, but may not necessarily reflect official Agency policy. The authors would also like  
626 to thank the Electric Power Research Institute (EPRI) for their support. M. Riva and J. D. Surratt  
627 wish to thank the Camille and Henry Dreyfus Postdoctoral Fellowship Program in  
628 Environmental Chemistry for their financial support. We thank J. Crouse and P. Wennberg  
629 from Caltech for gas-phase IEPOX data in SOAS-CTR and DC3, under support from NASA  
630 NNX12AC06G. We thank Lu Xu and Nga Lee Ng from Georgia Tech for providing data from  
631 their studies. We acknowledge funding from the UK Natural Environment Research Council  
632 through the OP3 and SAMBBA projects (Grant refs. NE/D002117/1 and NE/J010073/1).

633 **APPENDIX**

634 In addition to the preceding high resolution  $C_5H_6O^+$  data analysis, we also investigated unit mass  
635 resolution (UMR)  $m/z$  82 as a tracer of IEPOX-SOA. In addition to  $C_5H_6O^+$  ( $m/z$  82.0419), the  
636 reduced ion  $C_6H_{10}^+$  and oxygenated ion  $C_4H_2O_2^+$  often contribute signal to UMR  $m/z$  82. The  
637 average background level of  $f_{82}^{OA}$  ( $= m/z$  82/OA) is from  $4.3 \pm 0.9\%$  (0.01 to 10%) in studies  
638 strongly influenced by urban, biomass-burning and other anthropogenic POA, as shown in Fig.  
639 A1a – c. This value is higher than the high-resolution  $f_{C_5H_6O}^{OA-Bkg-UB}$  (1.7%) in the same studies.  
640 Background  $f_{82}^{OA}$  increases when OA is fresher (lower  $f_{44}$ ,  $f_{44}^{OA} = m/z$  44/OA) as shown in Fig A1d,  
641 and can be estimated as  $f_{82}^{OA} = 5.5 \times 10^{-3} - 8.2 \times 10^{-3} \times f_{44}^{OA}$  in areas strongly impacted by urban and  
642 biomass-burning emissions. The uncertainty of calculated  $f_{82}$  can be as high as 30% in the lower  
643 fresh OA plumes by considering the uncertainties from quantile average and linear regression.  
644 There are also some pure chemical species that exhibit high  $f_{82}$  values, as shown in Fig. A1c.  
645 These species include docosanol, eicosanol and oleic acid. However, none of these pure chemical  
646 species alone contributes substantially to ambient aerosol.

647 The probability density distributions of  $f_{82}^{OA}$  in studies strongly influenced by isoprene emissions  
648 are shown in Fig. A2a. The peaks ( $\sim 8.7 \pm 2.5\%$ ) are similar in SE US, pristine, polluted Amazon  
649 forest, Borneo forest to high resolution  $f_{C_5H_6O}^{OA}$  ( $\sim 6.5 \pm 2.2\%$ ), indicating  $C_5H_6O^+$  is the dominant  
650 ion at UMR  $m/z$  82 in these studies. Compared to the studies with strong urban and biomass-  
651 burning emissions, clear enhancements of  $f_{82}^{OA}$  in studies strongly influenced by isoprene  
652 emissions are still observed, but with less contrast than for in high resolution datasets (Fig. A2 –  
653 A3).

654 Figure 2Aa also shows the probability density distributions of  $f_{82}^{OA}$  at Rocky Mountain and  
655 European boreal forests (strongly influenced by monoterpene emissions). Those distributions

656 peak at ~5%, which are within the range (0.01 – 10%) of  $f_{82}^{OA}$  in aerosols strongly influenced by  
 657 urban and biomass-burning emissions. In the lab studies, most of  $f_{82}^{MT-SOA}$  (average  $6.7 \pm 2.2\%$ ;  
 658 range 4 – 11%) observed in the spectra of MT-SOA are also comparable to background  $f_{82}^{OA}$   
 659 levels (average  $4.3 \pm 0.9\%$ ; range 0.01–10%), and tend to be in the higher  $f_{82}^{OA}$  region from urban  
 660 and biomass-burning emissions. A linear regression line of  $f_{44}^{OA}$  vs  $f_{82}^{OA}$  for the Rocky Mountain  
 661 site ( $f_{82}^{OA} = 7.7 \times 10^{-3} - 0.019 \times f_{44}^{OA}$ ) is used to estimate the background  $f_{82}^{OA}$  from areas strongly  
 662 influenced by monoterpene emissions.

663 In summary, elevated  $f_{82}^{OA}$  in studies with high isoprene-emissions is observed. Pronounced  
 664  $f_{82}^{IEPOX-SOA}$  should be a key feature of IEPOX-SOA spectra. Thus IEPOX-SOA can be estimated  
 665 as Eq. (6) here:

$$666 \quad \text{IEPOX-SOA} = \frac{m_{82}^{\text{total}} - m_{82}^{\text{background}}}{f_{82}^{\text{IEPOX-SOA}} - f_{82}^{\text{OA-Bkg}}} = \frac{m_{82}^{\text{total}} - \text{OA}_{\text{mass}} \times f_{82}^{\text{OA-Bkg}}}{f_{82}^{\text{IEPOX-SOA}} - f_{82}^{\text{OA-Bkg}}}, \quad (6)$$

667 where  $f_{82}^{\text{IEPOX-SOA}}$  is 22% as obtained average (Fig. A3). In Eq. (4),  $f_{82}^{\text{OA-Bkg}}$  can be calculated  
 668 as a function of  $f_{44}^{OA}$  in studies strongly influenced by urban and biomass-burning emissions  
 669 ( $f_{82}^{OA} = 5.5 \times 10^{-3} - 8.2 \times 10^{-3} \times f_{44}^{OA}$ ) or monoterpene emissions ( $f_{82}^{OA} = 7.7 \times 10^{-3} - 0.019 \times f_{44}^{OA}$ ), as  
 670 discussed earlier.  $m_{82}^{\text{total}}$  and  $\text{OA}_{\text{mass}}$  are the measured ambient  $m/z$  82 and OA mass  
 671 concentrations by AMS. Because  $f_{82}$  in MT-SOA and OA from urban and biomass-burning  
 672 emissions cannot be separated, only one background value of  $f_{82}^{\text{OA-Bkg}}$  will be used in the UMR  
 673 method.

674 To test this UMR empirical method, we apply Eq. (6) to SOAS-CTR dataset, see Fig. A4. The  
 675 estimated IEPOX-SOA in SOAS-CTR from both background corrections (urban+biomass  
 676 burning vs monoterpene) both correlates well with  $\text{IEPOX-SOA}_{\text{PMF}}$  with  $R=0.97$  and  $R=0.98$ ,

677 respectively. The regression slopes between estimated fresh IEPOX-SOA vs IEPOX-SOA<sub>PMF</sub> are  
678 1.11 and 0.94, which are within 15% of 1:1 line. The deviation of estimated IEPOX-SOA from  
679 UMR by subtracting the background of MT-SOA influences is similar to that from HR in the  
680 SOAS dataset, indicating the UMR-based IEPOX-SOA estimation may perform as well as HR in  
681 areas with high IEPOX-SOA fractions. For areas with small IEPOX-SOA fractions, more  
682 uncertainties may exist in UMR calculation, e.g., there are wider variations of  $f_{82}^{OA-Bkg}$  from  
683 urban and biomass-burning emissions with oxidation level, whereas a smaller and less variable  
684  $f_{C_5H_6O}^{OA-Bkg}$  is found in HR. Overall,  $m/z$  82 in unit mass resolution data is also useful to estimate  
685 IEPOX-SOA. The different methods to estimate IEPOX-SOA may perform less well because of  
686 increased interferences from other ions at  $m/z$  82, however at locations with very high fractions  
687 of IEPOX-SOA such as SOAS-CTR, the UMR-based method performs well.

688

689 **References**

- 690 Aiken, A. C., Salcedo, D., Cubison, M. J., Huffman, J. A., DeCarlo, P. F., Ulbrich, I. M., Docherty, K. S.,  
691 Sueper, D., Kimmel, J. R., Worsnop, D. R., Trimborn, A., Northway, M., Stone, E. A., Schauer,  
692 J. J., Volkamer, R. M., Fortner, E., de Foy, B., Wang, J., Laskin, A., Shutthanandan, V., Zheng,  
693 J., Zhang, R., Gaffney, J., Marley, N. A., Paredes-Miranda, G., Arnott, W. P., Molina, L. T., Sosa,  
694 G., and Jimenez, J. L.: Mexico City aerosol analysis during MILAGRO using high resolution  
695 aerosol mass spectrometry at the urban supersite (T0) - Part 1: Fine particle composition and  
696 organic source apportionment, *Atmos Chem Phys*, 9, 6633-6653, 2009.
- 697 Alfarra, M.: Insights Into Atmospheric Organic Aerosols Using An Aerosol Mass Spectrometer, Doctor,  
698 Institute of Science and Technology, University of Manchester, Manchester, 2004.
- 699 Alfarra, M. R., Coe, H., Allan, J. D., Bower, K. N., Boudries, H., Canagaratna, M. R., Jimenez, J. L.,  
700 Jayne, J. T., Garforth, A. A., Li, S. M., and Worsnop, D. R.: Characterization of urban and rural  
701 organic particulate in the lower Fraser valley using two aerodyne aerosol mass spectrometers,  
702 *Atmos Environ*, 38, 5745-5758, DOI 10.1016/j.atmosenv.2004.01.054, 2004.
- 703 Allan, J. D., Morgan, W. T., Darbyshire, E., Flynn, M. J., Williams, P. I., Oram, D. E., Artaxo, P., Brito,  
704 J., Lee, J. D., and Coe, H.: Airborne observations of IEPOX-derived isoprene SOA in the  
705 Amazon during SAMBBA, *Atmos. Chem. Phys.*, 14, 11393-11407, 10.5194/acp-14-11393-2014,  
706 2014.
- 707 Anonymous\_Referee: Interactive comment on “Airborne observations of IEPOX-derived isoprene SOA  
708 in the Amazon during SAMBBA” by J. D. Allan et al., *Atmos. Chem. Phys. Discuss*, 14,, C5277–  
709 C5279, 2014.
- 710 Atkinson, R., and Arey, J.: Atmospheric Degradation of Volatile Organic Compounds, *Chem Rev*, 103,  
711 4605–4638, 10.1002/chin.200410285, 2003.
- 712 Bahreini, R., Keywood, M. D., Ng, N. L., Varutbangkul, V., Gao, S., Flagan, R. C., Seinfeld, J. H.,  
713 Worsnop, D. R., and Jimenez, J. L.: Measurements of secondary organic aerosol from oxidation  
714 of cycloalkenes, terpenes, and m-xylene using an Aerodyne aerosol mass spectrometer, *Environ*  
715 *Sci Technol*, 39, 5674-5688, Doi 10.1021/Es048061a, 2005.
- 716 Barth, M. C., Cantrell, C. A., Brune, W. H., Rutledge, S. A., Crawford, J. H., Huntrieser, H., Carey, L. D.,  
717 MacGorman, D., Weisman, M., Pickering, K. E., Bruning, E., Anderson, B., Apel, E.,  
718 Biggerstaff, M., Campos, T., Campuzano-Jost, P., Cohen, R., Crouse, J., Day, D. A., Diskin, G.,  
719 Flocke, F., Fried, A., Garland, C., Heikes, B., Honomichl, S., Hornbrook, R., Huey, L. G.,  
720 Jimenez, J. L., Lang, T., Lichtenstern, M., Mikoviny, T., Nault, B., O'Sullivan, D., Pan, L. L.,  
721 Peischl, J., Pollack, I., Richter, D., Riemer, D., Ryerson, T., Schlager, H., Clair, J. S., Walega, J.,  
722 Weibring, P., Weinheimer, A., Wennberg, P., Wisthaler, A., Wooldridge, P. J., and Ziegler, C.:  
723 The Deep Convective Clouds and Chemistry (DC3) Field Campaign, *B. Am. Meteorol. Soc.*,  
724 published online first, doi:10.1175/bams-d-13-00290.1, 2014.
- 725 Boyd, C. M., Sanchez, J., Xu, L., Eugene, A. J., Nah, T., Tuet, W. Y., Guzman, M. I., and Ng, N. L.:  
726 Secondary organic aerosol formation from the  $\beta$ -pinene+NO<sub>3</sub> system: effect of humidity and  
727 peroxy radical fate, *Atmos. Chem. Phys.*, 15, 7497-7522, 10.5194/acp-15-7497-2015, 2015.
- 728 Budisulistiorini, S. H., Canagaratna, M. R., Croteau, P. L., Marth, W. J., Baumann, K., Edgerton, E. S.,  
729 Shaw, S. L., Knipping, E. M., Worsnop, D. R., Jayne, J. T., Gold, A., and Surratt, J. D.: Real-  
730 Time Continuous Characterization of Secondary Organic Aerosol Derived from Isoprene  
731 Epoxydiols in Downtown Atlanta, Georgia, Using the Aerodyne Aerosol Chemical Speciation  
732 Monitor, *Environ Sci Technol*, 47, 5686-5694, 10.1021/es400023n, 2013.
- 733 Budisulistiorini, S. H., Li, X., Bairai, S. T., Renfro, J., Liu, Y., Liu, Y. J., McKinney, K. A., Martin, S. T.,  
734 McNeill, V. F., Pye, H. O. T., Nenes, A., Neff, M. E., Stone, E. A., Mueller, S., Knote, C., Shaw,  
735 S. L., Zhang, Z., Gold, A., and Surratt, J. D.: Examining the effects of anthropogenic emissions  
736 on isoprene-derived secondary organic aerosol formation during the 2013 Southern Oxidant and  
737 Aerosol Study (SOAS) at the Look Rock, Tennessee ground site, *Atmos. Chem. Phys.*, 15, 8871-  
738 8888, 10.5194/acp-15-8871-2015, 2015.



739 Canagaratna, M. R., Jayne, J. T., Ghertner, D. A., Herndon, S., Shi, Q., Jimenez, J. L., Silva, P. J.,  
740 Williams, P., Lanni, T., Drewnick, F., Demerjian, K. L., Kolb, C. E., and Worsnop, D. R.: Chase  
741 studies of particulate emissions from in-use New York City vehicles, *Aerosol Sci Tech*, 38, 555-  
742 573, Doi 10.1080/02786820490465504, 2004.

743 Canagaratna, M. R., Jimenez, J. L., Kroll, J. H., Chen, Q., Kessler, S. H., Massoli, P., Hildebrandt Ruiz,  
744 L., Fortner, E., Williams, L. R., Wilson, K. R., Surratt, J. D., Donahue, N. M., Jayne, J. T., and  
745 Worsnop, D. R.: Elemental ratio measurements of organic compounds using aerosol mass  
746 spectrometry: characterization, improved calibration, and implications, *Atmos. Chem. Phys.*, 15,  
747 253-272, 10.5194/acp-15-253-2015, 2015.

748 Carbone, S., De Brito, J. F., Andreae, M., Pöhlker, C., Chi, X., Saturno, J., Barbosa, H., and Artaxo, P.:  
749 Preliminary characterization of submicron secondary aerosol in the amazon forest – ATTO  
750 station, In prep., 2015.

751 Chang, R. Y. W., Leck, C., Graus, M., Müller, M., Paatero, J., Burkhardt, J. F., Stohl, A., Orr, L. H.,  
752 Hayden, K., Li, S. M., Hansel, A., Tjernström, M., Leaitch, W. R., and Abbatt, J. P. D.: Aerosol  
753 composition and sources in the central Arctic Ocean during ASCOS, *Atmos. Chem. Phys.*, 11,  
754 10619-10636, 10.5194/acp-11-10619-2011, 2011.

755 Chen, Q., Liu, Y., Donahue, N. M., Shilling, J. E., and Martin, S. T.: Particle-Phase Chemistry of  
756 Secondary Organic Material: Modeled Compared to Measured O:C and H:C Elemental Ratios  
757 Provide Constraints, *Environ Sci Technol*, 45, 4763-4770, 10.1021/es104398s, 2011.

758 Chen, Q., Farmer, D. K., Rizzo, L. V., Pauliquevis, T., Kuwata, M., Karl, T. G., Guenther, A., Allan, J.  
759 D., Coe, H., Andreae, M. O., Pöschl, U., Jimenez, J. L., Artaxo, P., and Martin, S. T.: Fine-mode  
760 organic mass concentrations and sources in the Amazonian wet season (AMAZE-08), *Atmos.*  
761 *Chem. Phys. Discuss.*, 14, 16151-16186, 10.5194/acpd-14-16151-2014, 2014.

762 Chhabra, P. S., Ng, N. L., Canagaratna, M. R., Corrigan, A. L., Russell, L. M., Worsnop, D. R., Flagan,  
763 R. C., and Seinfeld, J. H.: Elemental composition and oxidation of chamber organic aerosol,  
764 *Atmos. Chem. Phys.*, 11, 8827-8845, 10.5194/acp-11-8827-2011, 2011.

765 Coggon, M. M., Sorooshian, A., Wang, Z., Metcalf, A. R., Frossard, A. A., Lin, J. J., Craven, J. S.,  
766 Nenes, A., Jonsson, H. H., Russell, L. M., Flagan, R. C., and Seinfeld, J. H.: Ship impacts on the  
767 marine atmosphere: insights into the contribution of shipping emissions to the properties of  
768 marine aerosol and clouds, *Atmos. Chem. Phys.*, 12, 8439–8458, doi:10.5194/acp-12-8439-2012,  
769 2012.

770 Cole-Filipiak, N. C., O'Connor, A. E., and Elrod, M. J.: Kinetics of the Hydrolysis of Atmospherically  
771 Relevant Isoprene-Derived Hydroxy Epoxides, *Environ Sci Technol*, 44, 6718-6723,  
772 10.1021/es1019228, 2010.

773 Corrigan, A. L., Russell, L. M., Takahama, S., Äijälä, M., Ehn, M., Junninen, H., Rinne, J., Petäjä, T.,  
774 Kulmala, M., Vogel, A. L., Hoffmann, T., Ebben, C. J., Geiger, F. M., Chhabra, P., Seinfeld, J.  
775 H., Worsnop, D. R., Song, W., Auld, J., and Williams, J.: Biogenic and biomass burning organic  
776 aerosol in a boreal forest at Hyytiälä, Finland, during HUMPPA-COPEC 2010, *Atmos. Chem.*  
777 *Phys.*, 13, 12233-12256, 10.5194/acp-13-12233-2013, 2013.

778 Crippa, M., El Haddad, I., Slowik, J. G., DeCarlo, P. F., Mohr, C., Heringa, M. F., Chirico, R., Marchand,  
779 N., Sciare, J., Baltensperger, U., and Prévôt, A. S. H.: Identification of marine and continental  
780 aerosol sources in Paris using high resolution aerosol mass spectrometry, *J. Geophys. Res.-*  
781 *Atmos.*, 118, 1950–1963, doi:10.1002/jgrd.50151, 2013.

782 Cubison, M. J., Ortega, A. M., Hayes, P. L., Farmer, D. K., Day, D., Lechner, M. J., Brune, W. H., Apel,  
783 E., Diskin, G. S., Fisher, J. A., Fuelberg, H. E., Hecobian, A., Knapp, D. J., Mikoviny, T.,  
784 Riemer, D., Sachse, G. W., Sessions, W., Weber, R. J., Weinheimer, A. J., Wisthaler, A., and  
785 Jimenez, J. L.: Effects of aging on organic aerosol from open biomass burning smoke in aircraft  
786 and laboratory studies, *Atmos. Chem. Phys.*, 11, 12049-12064, 10.5194/acp-11-12049-2011,  
787 2011.

788 de Sá, S. S., Palm, B. B., Campuzano-Jost, P., Day, D. A., Hu, W., Newburn, M. K., Brito, J., Liu, Y.,  
789 Isaacman-VanWertz, G., Yee, L. D., Goldstein, A. H., Artaxo, P., Souza, R., Manzi, A., Jimenez,  
790 J. L., Alexander, M. L., and Martin, S. T., In prep., 2015.

791 DeCarlo, P. F., Kimmel, J. R., Trimborn, A., Northway, M. J., Jayne, J. T., Aiken, A. C., Gonin, M.,  
792 Fuhrer, K., Horvath, T., Docherty, K. S., Worsnop, D. R., and Jimenez, J. L.: Field-deployable,  
793 high-resolution, time-of-flight aerosol mass spectrometer, *Anal Chem*, 78, 8281-8289, Doi  
794 10.1021/Ac061249n, 2006.

795 Docherty, K. S., Aiken, A. C., Huffman, J. A., Ulbrich, I. M., DeCarlo, P. F., Sueper, D., Worsnop, D. R.,  
796 Snyder, D. C., Peltier, R. E., Weber, R. J., Grover, B. D., Eatough, D. J., Williams, B. J.,  
797 Goldstein, A. H., Ziemann, P. J., and Jimenez, J. L.: The 2005 Study of Organic Aerosols at  
798 Riverside (SOAR-1): instrumental intercomparisons and fine particle composition, *Atmos. Chem.*  
799 *Phys.*, 11, 12387-12420, 10.5194/acp-11-12387-2011, 2011.

800 Dunlea, E. J., DeCarlo, P. F., Aiken, A. C., Kimmel, J. R., Peltier, R. E., Weber, R. J., Tomlinson, J.,  
801 Collins, D. R., Shinozuka, Y., McNaughton, C. S., Howell, S. G., Clarke, A. D., Emmons, L. K.,  
802 Apel, E. C., Pfister, G. G., van Donkelaar, A., Martin, R. V., Millet, D. B., Heald, C. L., and  
803 Jimenez, J. L.: Evolution of Asian aerosols during transpacific transport in INTEX-B, *Atmos*  
804 *Chem Phys*, 9, 7257-7287, 2009.

805 Dzepina, K., Arey, J., Marr, L. C., Worsnop, D. R., Salcedo, D., Zhang, Q., Onasch, T. B., Molina, L. T.,  
806 Molina, M. J., and Jimenez, J. L.: Detection of particle-phase polycyclic aromatic hydrocarbons  
807 in Mexico City using an aerosol mass spectrometer, *Int J Mass Spectrom*, 263, 152-170, DOI  
808 10.1016/j.ijms.2007.01.010, 2007.

809 Ebben, C. J., Martinez, I. S., Shrestha, M., Buchbinder, A. M., Corrigan, A. L., Guenther, A., Karl, T.,  
810 Petäjä, T., Song, W. W., Zorn, S. R., Artaxo, P., Kulmala, M., Martin, S. T., Russell, L. M.,  
811 Williams, J., and Geiger, F. M.: Contrasting organic aerosol particles from boreal and tropical  
812 forests during HUMPPA-COPEC-2010 and AMAZE-08 using coherent vibrational spectroscopy,  
813 *Atmos. Chem. Phys.*, 11, 10317-10329, 10.5194/acp-11-10317-2011, 2011.

814 Eddingsaas, N. C., VanderVelde, D. G., and Wennberg, P. O.: Kinetics and Products of the Acid-  
815 Catalyzed Ring-Opening of Atmospherically Relevant Butyl Epoxy Alcohols, *The Journal of*  
816 *Physical Chemistry A*, 114, 8106-8113, 10.1021/jp103907c, 2010.

817 Fröhlich, R., Crenn, V., Setyan, A., Belis, C. A., Canonaco, F., Favez, O., Riffault, V., Slowik, J. G., Aas,  
818 W., Aijälä, M., Alastuey, A., Artiñano, B., Bonnaire, N., Bozzetti, C., Bressi, M., Carbone, C.,  
819 Coz, E., Croteau, P. L., Cubison, M. J., Esser-Gietl, J. K., Green, D. C., Gros, V., Heikkinen, L.,  
820 Herrmann, H., Jayne, J. T., Lunder, C. R., Minguillón, M. C., Močnik, G., O'Dowd, C. D.,  
821 Ovadnevaite, J., Petralia, E., Poulain, L., Priestman, M., Ripoll, A., Sarda-Estève, R.,  
822 Wiedensohler, A., Baltensperger, U., Sciare, J., and Prévôt, A. S. H.: ACTRIS ACSM  
823 intercomparison – Part 2: Intercomparison of ME-2 organic source apportionment results from 15  
824 individual, co-located aerosol mass spectrometers, *Atmos. Meas. Tech.*, 8, 2555-2576,  
825 10.5194/amt-8-2555-2015, 2015.

826 Froyd, K. D., Murphy, S. M., Murphy, D. M., de Gouw, J. A., Eddingsaas, N. C., and Wennberg, P. O.:  
827 Contribution of isoprene-derived organosulfates to free tropospheric aerosol mass, *P. Natl. Acad.*  
828 *Sci. USA*, 107, 21360–21365, doi:10.1073/pnas.1012561107, 2010.

829 Fry, J. L., Draper, D. C., Zarzana, K. J., Campuzano-Jost, P., Day, D. A., Jimenez, J. L., Brown, S. S.,  
830 Cohen, R. C., Kaser, L., Hansel, A., Cappellin, L., Karl, T., Hodzic Roux, A., Turnipseed, A.,  
831 Cantrell, C., Lefer, B. L., and Grossberg, N.: Observations of gas- and aerosol-phase organic  
832 nitrates at BEACHON-RoMBAS 2011, *Atmos. Chem. Phys.*, 13, 8585-8605, 10.5194/acp-13-  
833 8585-2013, 2013.

834 Fry, J. L., Draper, D. C., Barsanti, K. C., Smith, J. N., Ortega, J., Winkler, P. M., Lawler, M. J., Brown, S.  
835 S., Edwards, P. M., Cohen, R. C., and Lee, L.: Secondary Organic Aerosol Formation and  
836 Organic Nitrate Yield from NO<sub>3</sub> Oxidation of Biogenic Hydrocarbons, *Environ. Sci. Technol*, 48,  
837 11944–11953, doi:10.1021/es502204x, 2014.

838 Gaston, C. J., Riedel, T. P., Zhang, Z., Gold, A., Surratt, J. D., and Thornton, J. A.: Reactive Uptake of an  
839 Isoprene-Derived Epoxydiol to Submicron Aerosol Particles, *Environ. Sci. Technol.*, 48, 11178–  
840 11186, doi:10.1021/es5034266, 2014.

841 Guenther, A. B., Jiang, X., Heald, C. L., Sakulyanontvittaya, T., Duhl, T., Emmons, L. K., and Wang, X.:  
842 The Model of Emissions of Gases and Aerosols from Nature version 2.1 (MEGAN2.1): an  
843 extended and updated framework for modeling biogenic emissions, *Geosci. Model Dev.*, 5, 1471-  
844 1492, 10.5194/gmd-5-1471-2012, 2012.

845 Hayes, P. L., Ortega, A. M., Cubison, M. J., Froyd, K. D., Zhao, Y., Cliff, S. S., Hu, W. W., Toohey, D.  
846 W., Flynn, J. H., Lefer, B. L., Grossberg, N., Alvarez, S., Rappenglück, B., Taylor, J. W., Allan,  
847 J. D., Holloway, J. S., Gilman, J. B., Kuster, W. C., de Gouw, J. A., Massoli, P., Zhang, X., Liu,  
848 J., Weber, R. J., Corrigan, A. L., Russell, L. M., Isaacman, G., Worton, D. R., Kreisberg, N. M.,  
849 Goldstein, A. H., Thalman, R., Waxman, E. M., Volkamer, R., Lin, Y. H., Surratt, J. D.,  
850 Kleindienst, T. E., Offenberg, J. H., Dusanter, S., Griffith, S., Stevens, P. S., Brioude, J.,  
851 Angevine, W. M., and Jimenez, J. L.: Organic aerosol composition and sources in Pasadena,  
852 California, during the 2010 CalNex campaign, *Journal of Geophysical Research: Atmospheres*,  
853 118, 9233-9257, 10.1002/jgrd.50530, 2013.

854 He, L. Y., Lin, Y., Huang, X. F., Guo, S., Xue, L., Su, Q., Hu, M., Luan, S. J., and Zhang, Y. H.:  
855 Characterization of high-resolution aerosol mass spectra of primary organic aerosol emissions  
856 from Chinese cooking and biomass burning, *Atmos. Chem. Phys.*, 10, 11535-11543,  
857 10.5194/acp-10-11535-2010, 2010.

858 Hersey, S. P., Craven, J. S., Schilling, K. A., Metcalf, A. R., Sorooshian, A., Chan, M. N., Flagan, R. C.,  
859 and Seinfeld, J. H.: The Pasadena Aerosol Characterization Observatory (PACO): chemical and  
860 physical analysis of the Western Los Angeles basin aerosol, *Atmos. Chem. Phys.*, 11, 7417-7443,  
861 10.5194/acp-11-7417-2011, 2011.

862 Hu, D., Bian, Q., Li, T. W. Y., Lau, A. K. H., and Yu, J. Z.: Contributions of isoprene, monoterpenes,  $\beta$ -  
863 caryophyllene, and toluene to secondary organic aerosols in Hong Kong during the summer of  
864 2006, *Journal of Geophysical Research: Atmospheres*, 113, D22206, 10.1029/2008jd010437,  
865 2008.

866 Hu, W., Hu, M., Hu, W., Jimenez, J.-L., Yuan, B., Chen, W., Wang, M., Wu, Y., Wang, Z., Chen, C.,  
867 Peng, J., Shao, M., and Zeng, L.: Chemical composition, sources and aging process of sub-micron  
868 aerosols in Beijing: contrast between summer and winter, submitted, 2015.

869 Hu, W. W., Hu, M., Yuan, B., Jimenez, J. L., Tang, Q., Peng, J. F., Hu, W., Shao, M., Wang, M., Zeng,  
870 L. M., Wu, Y. S., Gong, Z. H., Huang, X. F., and He, L. Y.: Insights on organic aerosol aging and  
871 the influence of coal combustion at a regional receptor site of central eastern China, *Atmos.*  
872 *Chem. Phys.*, 13, 10095-10112, 10.5194/acp-13-10095-2013, 2013.

873 Huang, X. F., He, L. Y., Hu, M., Canagaratna, M. R., Sun, Y., Zhang, Q., Zhu, T., Xue, L., Zeng, L. W.,  
874 Liu, X. G., Zhang, Y. H., Jayne, J. T., Ng, N. L., and Worsnop, D. R.: Highly time-resolved  
875 chemical characterization of atmospheric submicron particles during 2008 Beijing Olympic  
876 Games using an Aerodyne High-Resolution Aerosol Mass Spectrometer, *Atmos Chem Phys*, 10,  
877 8933-8945, DOI 10.5194/acp-10-8933-2010, 2010.

878 Isaacman, G., Kreisberg, N. M., Yee, L. D., Worton, D. R., Chan, A. W. H., Moss, J. A., Hering, S. V.,  
879 and Goldstein, A. H.: Online derivatization for hourly measurements of gas- and particle-phase  
880 semi-volatile oxygenated organic compounds by thermal desorption aerosol gas chromatography  
881 (SV-TAG), *Atmos. Meas. Tech.*, 7, 4417-4429, 10.5194/amt-7-4417-2014, 2014.

882 Jacobs, M. I., Burke, W. J., and Elrod, M. J.: Kinetics of the reactions of isoprene-derived  
883 hydroxynitrates: gas phase epoxide formation and solution phase hydrolysis, *Atmos. Chem.*  
884 *Phys.*, 14, 8933-8946, 10.5194/acp-14-8933-2014, 2014.

885 Jimenez-Group: Aerosol Mass Spectrometer Web Mass Spectral Database, High-Resolution  
886 AMS Spectra, available at: <http://cires.colorado.edu/jimenez-group/HRAMSsd/> (last access:  
887 15 December 2014); unit mass resolution spectra, available at: [http://cires.colorado.edu/](http://cires.colorado.edu/jimenez-group/AMSsd/)  
888 [jimenez-group/AMSsd/](http://cires.colorado.edu/jimenez-group/AMSsd/) (last access: 15 December 2014), University of Colorado, Boulder,

889 2015.  
890 Jimenez, J. L., Jayne, J. T., Shi, Q., Kolb, C. E., Worsnop, D. R., Yourshaw, I., Seinfeld, J. H., Flagan, R.  
891 C., Zhang, X. F., Smith, K. A., Morris, J. W., and Davidovits, P.: Ambient aerosol sampling  
892 using the Aerodyne Aerosol Mass Spectrometer, *J. Geophys. Res.-Atmos.*, 108, 8425,  
893 doi:10.1029/2001jd001213, 2003.  
894 Kang, E., Root, M. J., Toohey, D. W., and Brune, W. H.: Introducing the concept of Potential Aerosol  
895 Mass (PAM), *Atmos. Chem. Phys.*, 7, 5727-5744, 10.5194/acp-7-5727-2007, 2007.  
896 Karl, T., Guenther, A., Turnipseed, A., Tyndall, G., Artaxo, P., and Martin, S.: Rapid formation of  
897 isoprene photo-oxidation products observed in Amazonia, *Atmos. Chem. Phys.*, 9, 7753-7767,  
898 10.5194/acp-9-7753-2009, 2009.  
899 Karl, T., Kaser, L., and Turnipseed, A.: Eddy covariance measurements of isoprene and 232-MBO based  
900 on NO<sup>+</sup> time-of-flight mass spectrometry, *Int J Mass Spectrom*, 365–366, 15-19, 2014.  
901 Kaser, L., Karl, T., Schnitzhofer, R., Graus, M., Herdinger-Blatt, I. S., DiGangi, J. P., Sive, B.,  
902 Turnipseed, A., Hornbrook, R. S., Zheng, W., Flocke, F. M., Guenther, A., Keutsch, F. N., Apel,  
903 E., and Hansel, A.: Comparison of different real time VOC measurement techniques in a  
904 ponderosa pine forest, *Atmos. Chem. Phys.*, 13, 2893-2906, 10.5194/acp-13-2893-2013, 2013.  
905 Katrib, Y., Martin, S. T., Hung, H.-M., Rudich, Y., Zhang, H., Slowik, J. G., Davidovits, P., Jayne, J. T.,  
906 and Worsnop, D. R.: Products and Mechanisms of Ozone Reactions with Oleic Acid for Aerosol  
907 Particles Having Core–Shell Morphologies, *The Journal of Physical Chemistry A*, 108, 6686-  
908 6695, 10.1021/jp049759d, 2004.  
909 Krechmer, J. E., Coggon, M. M., Massoli, P., Nguyen, T. B., Crounse, J. D., Hu, W., Day, D. A., Tyndall,  
910 G. S., Henze, D. K., Rivera-Rios, J. C., Nowak, J. B., Kimmel, J. R., Mauldin, R. L., Stark, H.,  
911 Jayne, J. T., Sipilä, M., Junninen, H., St. Clair, J. M., Zhang, X., Feiner, P. A., Zhang, L., Miller,  
912 D. O., Brune, W. H., Keutsch, F. N., Wennberg, P. O., Seinfeld, J. H., Worsnop, D. R., Jimenez,  
913 J. L., and Canagaratna, M. R.: Formation of Low Volatility Organic Compounds and Secondary  
914 Organic Aerosol from Isoprene Hydroxyhydroperoxide Low-NO Oxidation, *Environ Sci*  
915 *Technol*, 10.1021/acs.est.5b02031, 2015.  
916 Kroll, J. H., Ng, N. L., Murphy, S. M., Flagan, R. C., and Seinfeld, J. H.: Secondary organic aerosol  
917 formation from isoprene photooxidation, *Environ Sci Technol*, 40, 1869-1877, Doi  
918 10.1021/Es0524301, 2006.  
919 Kuwata, M., Liu, Y., McKinney, K., and Martin, S. T.: Physical state and acidity of inorganic sulfate can  
920 regulate the production of secondary organic material from isoprene photooxidation products,  
921 *Phys Chem Chem Phys*, 17, 5670-5678, 10.1039/c4cp04942j, 2015.  
922 Lanz, V. A., Alfarra, M. R., Baltensperger, U., Buchmann, B., Hueglin, C., and Prevot, A. S. H.: Source  
923 apportionment of submicron organic aerosols at an urban site by factor analytical modelling of  
924 aerosol mass spectra, *Atmos Chem Phys*, 7, 1503-1522, 2007.  
925 Levin, E. J. T., Prenni, A. J., Palm, B. B., Day, D. A., Campuzano-Jost, P., Winkler, P. M., Kreidenweis,  
926 S. M., DeMott, P. J., Jimenez, J. L., and Smith, J. N.: Size-resolved aerosol composition and its  
927 link to hygroscopicity at a forested site in Colorado, *Atmos. Chem. Phys.*, 14, 2657-2667,  
928 10.5194/acp-14-2657-2014, 2014.  
929 Lewandowski, M., Piletic, I. R., Kleindienst, T. E., Offenber, J. H., Beaver, M. R., Jaoui, M., Docherty,  
930 K. S., and Edney, E. O.: Secondary organic aerosol characterisation at field sites across the  
931 United States during the spring–summer period, *International Journal of Environmental*  
932 *Analytical Chemistry*, 93, 1084-1103, 10.1080/03067319.2013.803545, 2013.  
933 Li, R., Palm, B. B., Borbon, A., Graus, M., Warneke, C., Ortega, A. M., Day, D. A., Brune, W. H.,  
934 Jimenez, J. L., and de Gouw, J. A.: Laboratory Studies on Secondary Organic Aerosol Formation  
935 from Crude Oil Vapors, *Environ Sci Technol*, 47, 12566-12574, 10.1021/es402265y, 2013.  
936 Li, Y. J., Yeung, J. W. T., Leung, T. P. I., Lau, A. P. S., and Chan, C. K.: Characterization of Organic  
937 Particles from Incense Burning Using an Aerodyne High-Resolution Time-of-Flight Aerosol  
938 Mass Spectrometer, *Aerosol Sci Tech*, 46, 654-665, 10.1080/02786826.2011.653017, 2011.

939 Liao, J., Froyd, K. D., Murphy, D. M., Keutsch, F. N., Yu, G., Wennberg, P. O., Clair, J. S., Crouse, J.  
940 D., Wisthaler, A., Mikoviny, T., Ryerson, T. B., Pollack, I. B., Peischl, J. L., Collett, J., Jimenez,  
941 J. L., Campuzano-Jost, P., Day, D. A., Hu, W. W., Anderson, B. E., Ziemba, L. D., Blake, D. R.,  
942 Meinardi, S., and Diskin, G.: Airborne organosulfates measurements over the continental US, *J*  
943 *Geophys Res-Atmos*, 120, 2990-3005, 2014.

944 Liggio, J., Li, S. M., and McLaren, R.: Reactive uptake of glyoxal by particulate matter, *J Geophys Res-*  
945 *Atmos*, 110, D10304, doi:10.1029/2004jd005113, 2005.

946 Lin, Y.-H., Zhang, Z., Docherty, K. S., Zhang, H., Budisulistiorini, S. H., Rubitschun, C. L., Shaw, S. L.,  
947 Knipping, E. M., Edgerton, E. S., Kleindienst, T. E., Gold, A., and Surratt, J. D.: Isoprene  
948 Epoxydiols as Precursors to Secondary Organic Aerosol Formation: Acid-Catalyzed Reactive  
949 Uptake Studies with Authentic Compounds, *Environ Sci Technol*, 46, 250-258,  
950 10.1021/es202554c, 2012.

951 Lin, Y.-H., Budisulistiorini, S. H., Chu, K., Siejack, R. A., Zhang, H., Riva, M., Zhang, Z., Gold, A.,  
952 Kautzman, K. E., and Surratt, J. D.: Light-Absorbing Oligomer Formation in Secondary Organic  
953 Aerosol from Reactive Uptake of Isoprene Epoxydiols, *Environ Sci Technol*, 48, 12012-12021,  
954 10.1021/es503142b, 2014.

955 Liu, Y., Kuwata, M., Strick, B. F., Thomson, R. J., Geiger, F. M., McKinney, K., and Martin, S. T.:  
956 Uptake of Epoxydiol Isomers Accounts for Half of the Particle-Phase Material Produced from  
957 Isoprene Photooxidation via the HO<sub>2</sub> pathway, *Environ Sci Technol*, 49, 250-258,  
958 10.1021/es5034298, 2014.

959 Loza, C. L., Chhabra, P. S., Yee, L. D., Craven, J. S., Flagan, R. C., and Seinfeld, J. H.: Chemical aging  
960 of m-xylene secondary organic aerosol: laboratory chamber study, *Atmos. Chem. Phys.*, 12, 151-  
961 167, 10.5194/acp-12-151-2012, 2012.

962 Mael, L. E., Jacobs, M. I., and Elrod, M. J.: Organosulfate and Nitrate Formation and Reactivity from  
963 Epoxides Derived from 2-Methyl-3-buten-2-ol, *The Journal of Physical Chemistry A*,  
964 10.1021/jp510033s, 2014.

965 Mao, J., Paulot, F., Jacob, D. J., Cohen, R. C., Crouse, J. D., Wennberg, P. O., Keller, C. A., Hudman,  
966 R. C., Barkley, M. P., and Horowitz, L. W.: Ozone and organic nitrates over the eastern United  
967 States: Sensitivity to isoprene chemistry, *Journal of Geophysical Research: Atmospheres*, 118,  
968 2013JD020231, 10.1002/jgrd.50817, 2013.

969 Minguillón, M. C., Perron, N., Querol, X., Szidat, S., Fahrni, S. M., Alastuey, A., Jimenez, J. L., Mohr,  
970 C., Ortega, A. M., Day, D. A., Lanz, V. A., Wacker, L., Reche, C., Cusack, M., Amato, F., Kiss,  
971 G., Hoffer, A., Decesari, S., Moretti, F., Hillamo, R., Teinilä, K., Seco, R., Peñuelas, J., Metzger,  
972 A., Schallhart, S., Müller, M., Hansel, A., Burkhardt, J. F., Baltensperger, U., and Prévôt, A. S. H.:  
973 Fossil versus contemporary sources of fine elemental and organic carbonaceous particulate matter  
974 during the DAURE campaign in Northeast Spain, *Atmos. Chem. Phys.*, 11, 12067-12084,  
975 10.5194/acp-11-12067-2011, 2011.

976 Mohr, C., Huffman, J. A., Cubison, M. J., Aiken, A. C., Docherty, K. S., Kimmel, J. R., Ulbricht, I. M.,  
977 Hannigan, M., and Jimenez, J. L.: Characterization of Primary Organic Aerosol Emissions from  
978 Meat Cooking, Trash Burning, and Motor Vehicles with High-Resolution Aerosol Mass  
979 Spectrometry and Comparison with Ambient and Chamber Observations, *Environ Sci Technol*,  
980 43, 2443-2449, Doi 10.1021/Es8011518, 2009.

981 Mohr, C., DeCarlo, P. F., Heringa, M. F., Chirico, R., Slowik, J. G., Richter, R., Reche, C., Alastuey, A.,  
982 Querol, X., Seco, R., Peñuelas, J., Jiménez, J. L., Crippa, M., Zimmermann, R., Baltensperger,  
983 U., and Prévôt, A. S. H.: Identification and quantification of organic aerosol from cooking and  
984 other sources in Barcelona using aerosol mass spectrometer data, *Atmos. Chem. Phys.*, 12, 1649-  
985 1665, 10.5194/acp-12-1649-2012, 2012.

986 Ng, N. L., Chhabra, P. S., Chan, A. W. H., Surratt, J. D., Kroll, J. H., Kwan, A. J., McCabe, D. C.,  
987 Wennberg, P. O., Sorooshian, A., Murphy, S. M., Dalleska, N. F., Flagan, R. C., and Seinfeld, J.

988 H.: Effect of NO<sub>x</sub> level on secondary organic aerosol (SOA) formation from the photooxidation  
989 of terpenes, *Atmos Chem Phys*, 7, 5159-5174, 2007.

990 Ng, N. L., Kwan, A. J., Surratt, J. D., Chan, A. W. H., Chhabra, P. S., Sorooshian, A., Pye, H. O. T.,  
991 Crounse, J. D., Wennberg, P. O., Flagan, R. C., and Seinfeld, J. H.: Secondary organic aerosol  
992 (SOA) formation from reaction of isoprene with nitrate radicals (NO<sub>3</sub>), *Atmos. Chem. Phys.*, 8,  
993 4117-4140, 10.5194/acp-8-4117-2008, 2008.

994 Ng, N. L., Canagaratna, M. R., Jimenez, J. L., Chhabra, P. S., Seinfeld, J. H., and Worsnop, D. R.:  
995 Changes in organic aerosol composition with aging inferred from aerosol mass spectra, *Atmos.*  
996 *Chem. Phys.*, 11, 6465-6474, 10.5194/acp-11-6465-2011, 2011a.

997 Ng, N. L., Canagaratna, M. R., Jimenez, J. L., Zhang, Q., Ulbrich, I. M., and Worsnop, D. R.: Real-Time  
998 Methods for Estimating Organic Component Mass Concentrations from Aerosol Mass  
999 Spectrometer Data, *Environ Sci Technol*, 45, 910-916, 10.1021/es102951k, 2011b.

1000 Nguyen, T. B., Coggon, M. M., Bates, K. H., Zhang, X., Schwantes, R. H., Schilling, K. A., Loza, C. L.,  
1001 Flagan, R. C., Wennberg, P. O., and Seinfeld, J. H.: Organic aerosol formation from the reactive  
1002 uptake of isoprene epoxydiols (IEPOX) onto non-acidified inorganic seeds, *Atmos. Chem. Phys.*,  
1003 14, 3497-3510, 10.5194/acp-14-3497-2014, 2014.

1004 Nguyen, T. B., Crounse, J. D., Teng, A. P., St. Clair, J. M., Paulot, F., Wolfe, G. M., and Wennberg, P.  
1005 O.: Rapid deposition of oxidized biogenic compounds to a temperate forest, *Proceedings of the*  
1006 *National Academy of Sciences*, 112, E392-E401, 10.1073/pnas.1418702112, 2015.

1007 Ortega, A. M., Day, D. A., Cubison, M. J., Brune, W. H., Bon, D., de Gouw, J. A., and Jimenez, J. L.:  
1008 Secondary organic aerosol formation and primary organic aerosol oxidation from biomass-  
1009 burning smoke in a flow reactor during FLAME-3, *Atmos. Chem. Phys.*, 13, 11551-11571,  
1010 10.5194/acp-13-11551-2013, 2013.

1011 Ortega, J., Turnipseed, A., Guenther, A. B., Karl, T. G., Day, D. A., Gochis, D., Huffman, J. A., Prenni,  
1012 A. J., Levin, E. J. T., Kreidenweis, S. M., DeMott, P. J., Tobo, Y., Patton, E. G., Hodzic, A., Cui,  
1013 Y. Y., Harley, P. C., Hornbrook, R. S., Apel, E. C., Monson, R. K., Eller, A. S. D., Greenberg, J.  
1014 P., Barth, M. C., Campuzano-Jost, P., Palm, B. B., Jimenez, J. L., Aiken, A. C., Dubey, M. K.,  
1015 Geron, C., Offenberg, J., Ryan, M. G., Fornwalt, P. J., Pryor, S. C., Keutsch, F. N., DiGangi, J.  
1016 P., Chan, A. W. H., Goldstein, A. H., Wolfe, G. M., Kim, S., Kaser, L., Schnitzhofer, R., Hansel,  
1017 A., Cantrell, C. A., Mauldin, R. L., and Smith, J. N.: Overview of the Manitou Experimental  
1018 Forest Observatory: site description and selected science results from 2008 to 2013, *Atmos.*  
1019 *Chem. Phys.*, 14, 6345-6367, 10.5194/acp-14-6345-2014, 2014.

1020 Paulot, F., Crounse, J. D., Kjaergaard, H. G., Kroll, J. H., Seinfeld, J. H., and Wennberg, P. O.: Isoprene  
1021 photooxidation: new insights into the production of acids and organic nitrates, *Atmos. Chem.*  
1022 *Phys.*, 9, 1479-1501, 10.5194/acp-9-1479-2009, 2009a.

1023 Paulot, F., Crounse, J. D., Kjaergaard, H. G., Kürten, A., St. Clair, J. M., Seinfeld, J. H., and Wennberg,  
1024 P. O.: Unexpected Epoxide Formation in the Gas-Phase Photooxidation of Isoprene, *Science*,  
1025 325, 730-733, 10.1126/science.1172910, 2009b.

1026 Phinney, L., Leaitch, W. R., Lohmann, U., Boudries, H., Worsnop, D. R., Jayne, J. T., Toom-Sauntry, D.,  
1027 Wadleigh, M., Sharma, S., and Shantz, N.: Characterization of the aerosol over the sub-arctic  
1028 north east Pacific Ocean, *Deep-Sea Res Pt II*, 53, 2410-2433, DOI 10.1016/j.dsr2.2006.05.044,  
1029 2006.

1030 Pye, H. O. T., Pinder, R. W., Piletic, I. R., Xie, Y., Capps, S. L., Lin, Y.-H., Surratt, J. D., Zhang, Z.,  
1031 Gold, A., Luecken, D. J., Hutzell, W. T., Jaoui, M., Offenberg, J. H., Kleindienst, T. E.,  
1032 Lewandowski, M., and Edney, E. O.: Epoxide Pathways Improve Model Predictions of Isoprene  
1033 Markers and Reveal Key Role of Acidity in Aerosol Formation, *Environ Sci Technol*, 47, 11056-  
1034 11064, 10.1021/es402106h, 2013.

1035 Robinson, N. H., Hamilton, J. F., Allan, J. D., Langford, B., Oram, D. E., Chen, Q., Docherty, K., Farmer,  
1036 D. K., Jimenez, J. L., Ward, M. W., Hewitt, C. N., Barley, M. H., Jenkin, M. E., Rickard, A. R.,  
1037 Martin, S. T., McFiggans, G., and Coe, H.: Evidence for a significant proportion of Secondary

1038 Organic Aerosol from isoprene above a maritime tropical forest, *Atmos. Chem. Phys.*, 11, 1039-  
1039 1050, 10.5194/acp-11-1039-2011, 2011.

1040 Saarikoski, S., Carbone, S., Decesari, S., Giulianelli, L., Angelini, F., Canagaratna, M., Ng, N. L.,  
1041 Trimborn, A., Facchini, M. C., Fuzzi, S., Hillamo, R., and Worsnop, D.: Chemical  
1042 characterization of springtime submicrometer aerosol in Po Valley, Italy, *Atmos. Chem. Phys.*,  
1043 12, 8401–8421, doi:10.5194/acp-12-8401-2012, 2012.

1044 Sage, A. M., Weitkamp, E. A., Robinson, A. L., and Donahue, N. M.: Evolving mass spectra of the  
1045 oxidized component of organic aerosol: results from aerosol mass spectrometer analyses of aged  
1046 diesel emissions, *Atmos. Chem. Phys.*, 8, 1139-1152, 10.5194/acp-8-1139-2008, 2008.

1047 Schneider, J., Weimer, S., Drewnick, F., Borrmann, S., Helas, G., Gwaze, P., Schmid, O., Andreae, M.  
1048 O., and Kirchner, U.: Mass spectrometric analysis and aerodynamic properties of various types of  
1049 combustion-related aerosol particles, *Int J Mass Spectrom*, 258, 37-49, DOI  
1050 10.1016/j.ijms.2006.07.008, 2006.

1051 Schneider, J., Freutel, F., Zorn, S. R., Chen, Q., Farmer, D. K., Jimenez, J. L., Martin, S. T.,  
1052 Artaxo, P., Wiedensohler, A., and Borrmann, S.: Mass-spectrometric identification of pri15  
1053 mary biological particle markers and application to pristine submicron aerosol measurements  
1054 in Amazonia, *Atmos. Chem. Phys.*, 11, 11415–11429, doi:10.5194/acp-11-11415-  
1055 2011, 2011.

1056 Setyan, A., Zhang, Q., Merkel, M., Knighton, W. B., Sun, Y., Song, C., Shilling, J. E., Onasch, T. B.,  
1057 Herndon, S. C., Worsnop, D. R., Fast, J. D., Zaveri, R. A., Berg, L. K., Wiedensohler, A.,  
1058 Flowers, B. A., Dubey, M. K., and Subramanian, R.: Characterization of submicron particles  
1059 influenced by mixed biogenic and anthropogenic emissions using high-resolution aerosol mass  
1060 spectrometry: results from CARES, *Atmos. Chem. Phys.*, 12, 8131-8156, 10.5194/acp-12-8131-  
1061 2012, 2012.

1062 Slowik, J. G., Brook, J., Chang, R. Y. W., Evans, G. J., Hayden, K., Jeong, C. H., Li, S. M., Liggio, J.,  
1063 Liu, P. S. K., McGuire, M., Mihele, C., Sjostedt, S., Vlasenko, A., and Abbatt, J. P. D.:  
1064 Photochemical processing of organic aerosol at nearby continental sites: contrast between urban  
1065 plumes and regional aerosol, *Atmos. Chem. Phys.*, 11, 2991-3006, 10.5194/acp-11-2991-2011,  
1066 2011.

1067 Surratt, J. D., Kroll, J. H., Kleindienst, T. E., Edney, E. O., Claeys, M., Sorooshian, A., Ng, N. L.,  
1068 Offenberg, J. H., Lewandowski, M., Jaoui, M., Flagan, R. C., and Seinfeld, J. H.: Evidence for  
1069 organosulfates in secondary organic aerosol, *Environ Sci Technol*, 41, 517-527, Doi  
1070 10.1021/Es062081q, 2007.

1071 Surratt, J. D., Chan, A. W. H., Eddingsaas, N. C., Chan, M., Loza, C. L., Kwan, A. J., Hersey, S. P.,  
1072 Flagan, R. C., Wennberg, P. O., and Seinfeld, J. H.: Reactive intermediates revealed in secondary  
1073 organic aerosol formation from isoprene, *Proceedings of the National Academy of Sciences*, 107,  
1074 6640-6645, 10.1073/pnas.0911114107, 2010.

1075 Takegawa, N., Miyakawa, T., Kawamura, K., and Kondo, Y.: Contribution of selected dicarboxylic and  
1076 omega-oxocarboxylic acids in ambient aerosol to the m/z 44 signal of an aerodyne aerosol mass  
1077 spectrometer, *Aerosol Sci Tech*, 41, 418-437, Doi 10.1080/02786820701203215, 2007.

1078 Ulbrich, I. M., Canagaratna, M. R., Zhang, Q., Worsnop, D. R., and Jimenez, J. L.: Interpretation of  
1079 organic components from Positive Matrix Factorization of aerosol mass spectrometric data,  
1080 *Atmos Chem Phys*, 9, 2891-2918, 2009.

1081 Wang, W., Kourtchev, I., Graham, B., Cafmeyer, J., Maenhaut, W., and Claeys, M.: Characterization of  
1082 oxygenated derivatives of isoprene related to 2-methyltetrols in Amazonian aerosols using  
1083 trimethylsilylation and gas chromatography/ion trap mass spectrometry, *Rapid Commun Mass  
1084 Sp*, 19, 1343-1351, 10.1002/rcm.1940, 2005.

1085 Weimer, S., Alfarra, M. R., Schreiber, D., Mohr, M., Prévôt, A. S. H., and Baltensperger, U.: Organic  
1086 aerosol mass spectral signatures from wood-burning emissions: Influence of burning conditions  
1087 and wood type, *J. Geophys. Res.*, 113, D10304, doi:10.1029/2007jd009309, 2008.

1088 Worton, D. R., Surratt, J. D., LaFranchi, B. W., Chan, A. W. H., Zhao, Y., Weber, R. J., Park, J.-H.,  
1089 Gilman, J. B., de Gouw, J., Park, C., Schade, G., Beaver, M., Clair, J. M. S., Crounse, J.,  
1090 Wennberg, P., Wolfe, G. M., Harrold, S., Thornton, J. A., Farmer, D. K., Docherty, K. S.,  
1091 Cubison, M. J., Jimenez, J.-L., Frossard, A. A., Russell, L. M., Kristensen, K., Glasius, M., Mao,  
1092 J., Ren, X., Brune, W., Browne, E. C., Pusede, S. E., Cohen, R. C., Seinfeld, J. H., and Goldstein,  
1093 A. H.: Observational Insights into Aerosol Formation from Isoprene, *Environ Sci Technol*, 47,  
1094 11403-11413, 10.1021/es4011064, 2013.

1095 Xu, L., Guo, H., Boyd, C. M., Klein, M., Bougiatioti, A., Cerully, K. M., Hite, J. R., Isaacman-VanWertz,  
1096 G., Kreisberg, N. M., Knote, C., Olson, K., Koss, A., Goldstein, A. H., Hering, S. V., de Gouw,  
1097 J., Baumann, K., Lee, S.-H., Nenes, A., Weber, R. J., and Ng, N. L.: Effects of anthropogenic  
1098 emissions on aerosol formation from isoprene and monoterpenes in the southeastern United  
1099 States, *Proceedings of the National Academy of Sciences*, 112, 37-42, 10.1073/pnas.1417609112,  
1100 2014.

1101 Xu, L., Suresh, S., Guo, H., Weber, R. J., and Ng, N. L.: Aerosol characterization over the southeastern  
1102 United States using high-resolution aerosol mass spectrometry: spatial and seasonal variation of  
1103 aerosol composition and sources with a focus on organic nitrates, *Atmos. Chem. Phys.*, 15, 7307-  
1104 7336, 10.5194/acp-15-7307-2015, 2015.

1105 Zhang, H., Worton, D. R., Lewandowski, M., Ortega, J., Rubitschun, C. L., Park, J.-H., Kristensen, K.,  
1106 Campuzano-Jost, P., Day, D. A., Jimenez, J. L., Jaoui, M., Offenberg, J. H., Kleindienst, T. E.,  
1107 Gilman, J., Kuster, W. C., de Gouw, J., Park, C., Schade, G. W., Frossard, A. A., Russell, L.,  
1108 Kaser, L., Jud, W., Hansel, A., Cappellin, L., Karl, T., Glasius, M., Guenther, A., Goldstein, A.  
1109 H., Seinfeld, J. H., Gold, A., Kamens, R. M., and Surratt, J. D.: Organosulfates as Tracers for  
1110 Secondary Organic Aerosol (SOA) Formation from 2-Methyl-3-Buten-2-ol (MBO) in the  
1111 Atmosphere, *Environ Sci Technol*, 46, 9437-9446, 10.1021/es301648z, 2012.

1112 Zhang, H., Zhang, Z., Cui, T., Lin, Y.-H., Bhathela, N. A., Ortega, J., Worton, D. R., Goldstein, A. H.,  
1113 Guenther, A., Jimenez, J. L., Gold, A., and Surratt, J. D.: Secondary Organic Aerosol Formation  
1114 via 2-Methyl-3-buten-2-ol Photooxidation: Evidence of Acid-Catalyzed Reactive Uptake of  
1115 Epoxides, *Environmental Science & Technology Letters*, 1, 242-247, 10.1021/ez500055f, 2014.

1116



1117 **Table 1.** Datasets used in this study<sup>a</sup>. Ranges or average plus standard deviation of  $f_{C_5H_6O}$  (high resolution) and  $f_{82}$  (unit mass  
1118 resolution) in different studies are also included.

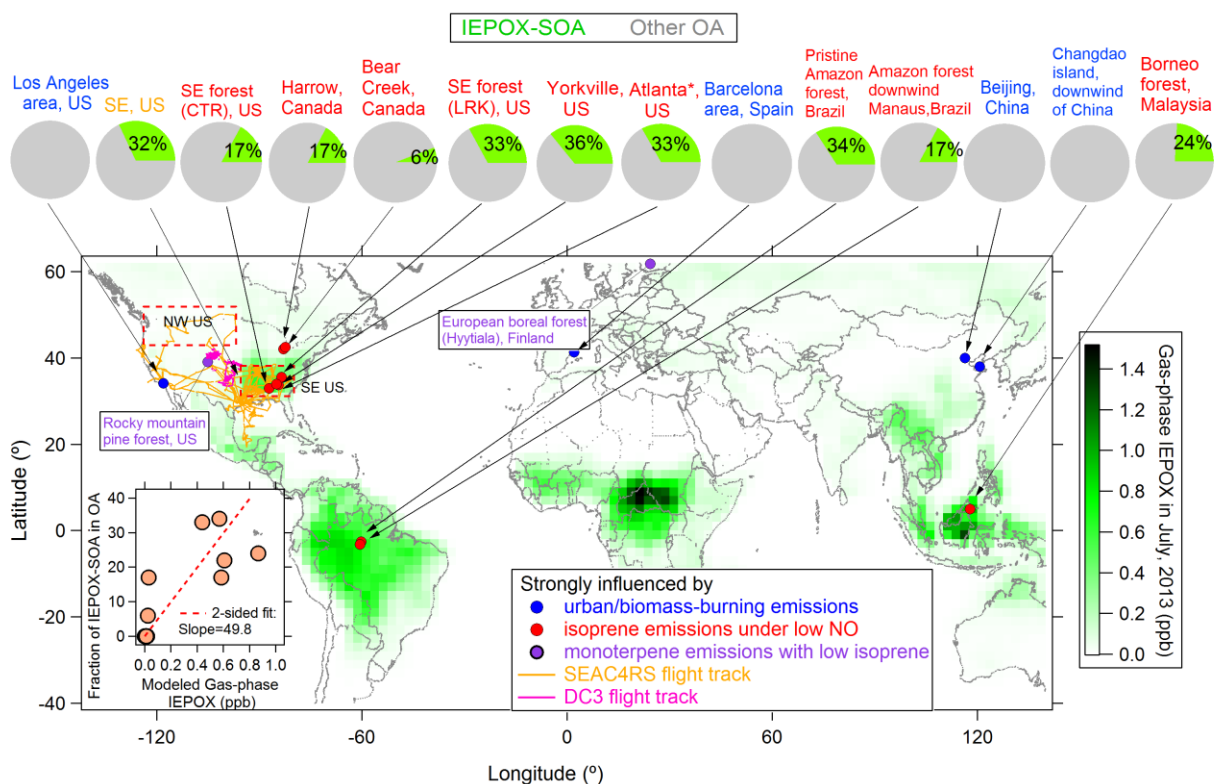
Name of datasets	Time Period	Site locations and descriptions	Campaign name	Ranges or average±std.de v. $f_{C_5H_6O}$ (‰)	Ranges or average±std.de v. $f_{82}$ (‰)	References
<b>Studies strongly-influenced by isoprene emissions under lower NO</b>						
SE US forest-CTR site	Jun-Jul, 2013	Centreville, AL,	SOAS	6.2±2.4	7.6±2.2	(1)
Pristine Amazon forest 2008, Brazil	Feb-Mar, 2008	Pristine rain forest site, TT34,	AMAZE-08	5.0±2.3	7.9±1.7	(2)
Amazon forest downwind Manaus, Brazil	Feb-Mar, 2014	T3 site, near Manacapuru	GoAmazon2014/5	6.9±1.6	7.1±1.0	(3)
Pristine Amazon forest 2014, Brazil	Aug-Dec, 2014	T0 site, ~150 km northeast of Manaus	GoAmazon2014/5	N/A	5.6±1.7	(4)
SE US	Aug-Sep, 2013	Aircraft measurement:	SEAC4RS	4.3±1.6	N/A	(5)
Borneo forest, Malaysia	Jun-Jul, 2008	Rain forest GAW station, Sabah, Malaysia	OP3	10±0.3	12.4±0.4	(6)
Atlanta, US	Aug-Sep, 2011	Urban JST site, Atlanta, Georgia, US	N/A	N/A	3.7±1.9	(7)
Atlanta (JST), US	May, 2012	Urban JST site, Atlanta, Georgia, US	N/A	3.3±0.9	N/A	(8)
Atlanta (GT), US	Aug, 2012	Urban Georgia Tech site, Georgia, US	N/A	5.4±1.9	N/A	(8)
Yorkville, US	July, 2012	Rural sites, 80km northwest of JST site, Georgia, US	N/A	7.7±2.2	N/A	(8)
Harrow, Canada	Jun-Jul, 2007	Harrow site, rural sites surrounded by farmland, Canada	BAQSMET	N/A	N/A	(9)
Bear Creek, Canada	Jun-Jul, 2007	Bear Creek site, wetlands area surrounded by farmland, Canada	BAQSMET	N/A	N/A	(9)
<b>Studies strongly-influenced by monoterpene emissions</b>						

Rocky mountain pine forest, CO, USA	Jul-Aug, 2011	Manitou Experimental Forest Observatory, CO,	BEACHON-RoMBAS	3.7±0.5	5.1±0.5	(10)
European Boreal forest, Finland	2008-2009	Hyytiala site in Pine forest, Finland	EUCAARI campaign	2.5±0.1 <sup>b</sup>	4.8±0.1 <sup>b</sup>	(11)
<b>Studies mixed-influenced by isoprene and monoterpene emissions</b>						
North American temperate, US	Aug-Sep, 2007	Blodgett Forest Ameriflux Site, CA, US	BEARPEX	4.0±<0.1 <sup>b</sup>	4.0±<0.1 <sup>b</sup>	(11)
<b>Studies strongly-influenced by urban emissions</b>						
Los Angeles area , CA, USA	May-Jun, 2010	Pasadena, US	CalNex	1.6±0.2	3.6±0.5	(12)
Beijing, China	Nov-Dec, 2010	Peking University, in NW of Beijing city, China	N/A	1.5±0.3	4.6±0.7	(13)
Changdao island, Downwind of China	Mar-Apr, 2011	Changdao island, China	CAPTAIN	1.6±0.2	3.8±0.5	(14)
Barcelona area, Spain	Feb-Mar, 2009	Montseny, Spain	DAURE	1.6±0.2	4.8±0.9	(15)
<b>Studies of biomass-burning smokes</b>						
BB Chamber study	Sep–Oct, 2009	Missoula, MO, USA	FLAME-3	1.9±0.6	5.9±1.4	(16)
Biomass burning plumes	Aug-Sep, 2013	All over US, aircraft measurement	SEAC4RS	1.8±0.5	N/A	(6)
Biomass burning plumes	May-Jun, 2011	All over US, aircraft measurement	DC-3	1.8±0.4	N/A	(17)
<b>Continental plumes</b>						
NW US	Aug-Sep, 2013	Aircraft measurement	SEAC4RS	1.7±0.3	N/A	(16)
Western US	May-Jun, 2011	Aircraft measurement	DC-3	1.9±0.6	N/A	(17)
<b>OA from specific sources</b>						
IEPOX-SOA from ambient PMF factors and chamber studies.				22±7	22±7	(18)
Isoprene derived non-IEPOX SOA (reaction with OH under conditions of high NO or low NO without seed not favorable for the reactive-uptake of IEPOX, reaction with NO <sub>3</sub> without seed)				<3	<3	(19)

Monoterpene-derived SOA	5.5±2.0	6.7±2.0	(20)
Other SOA (not from isoprene and monoterpene)	2.2±0.9	6.1±2.1	(21)
Cooking	1.5±0.8	8.2±1.1	(22)
Coal combustion	1.4-2.0	N/A	(23)
Vehicle emission	1.1±0.6	5.1±1.1	(24)
Biomass burning	2.3±0.7	4.3±1.5	(25)
Pure chemical species	0.7±1.0	4.0±5.5	(26)

1119 a- HR-ToF-AMS was used for all the campaigns except the Atlanta, US and Pristine Amazon forest 2014, Brazil using ACSM.  
1120 b- Standard error  
1121 (1) This study; (2) (Chen et al., 2014); (3) (de Sá et al., 2015); (4) (Carbone et al., 2015); (5)(Liao et al., 2014) ; (6) (Robinson et  
1122 al., 2011); (7) (Budisulistiorini et al., 2013); (8) (Xu et al., 2014;Xu et al., 2015) (9) (Slowik et al., 2011); (10) (Ortega et al., 2014);  
1123 (11) (Robinson et al., 2011); (12) (Hayes et al., 2013); (13) (Hu et al., 2015); (13) (Hu et al., 2013); (15) (Minguillón et al., 2011);  
1124 (16) (Ortega et al., 2013); (17) (Barth et al., 2014); (18) (Chhabra et al., 2011;Robinson et al., 2011;Budisulistiorini et al., 2013;Chen  
1125 et al., 2014;Liu et al., 2014;Kuwata et al., 2015); (19) (Kroll et al., 2006;Ng et al., 2008;Krechmer et al., 2015); (20) (Bahreini et al.,  
1126 2005;Chen et al., 2014;Boyd et al., 2015); (21) (Bahreini et al., 2005;Liggio et al., 2005;Chhabra et al., 2011;Loza et al., 2012); (22)  
1127 (Lanz et al., 2007;Mohr et al., 2009;He et al., 2010;Huang et al., 2010;Mohr et al., 2012;Crippa et al., 2013;Hu et al., 2015); (23)  
1128 (Hu et al., 2013;Hu et al., 2015); (24) (Canagaratna et al., 2004;Lanz et al., 2007;Sage et al., 2008;Aiken et al., 2009;Mohr et al.,  
1129 2009;Chang et al., 2011;Docherty et al., 2011;Hersey et al., 2011;Ng et al., 2011b;Coggon et al., 2012;Mohr et al., 2012;Saarikoski  
1130 et al., 2012;Setyan et al., 2012;Crippa et al., 2013); (25) (Schneider et al., 2006;Weimer et al., 2008;Aiken et al., 2009;He et al.,  
1131 2010;Ng et al., 2011b;Schneider et al., 2011;Mohr et al., 2012;Saarikoski et al., 2012;Crippa et al., 2013;Hu et al., 2013;Hu et al.,  
1132 2015); (26) (Alfarra, 2004;Katrib et al., 2004;Phinney et al., 2006;Dzepina et al., 2007;Takegawa et al., 2007;Aiken et al., 2009;Li et  
1133 al., 2011;Schneider et al., 2011)  
1134

1135

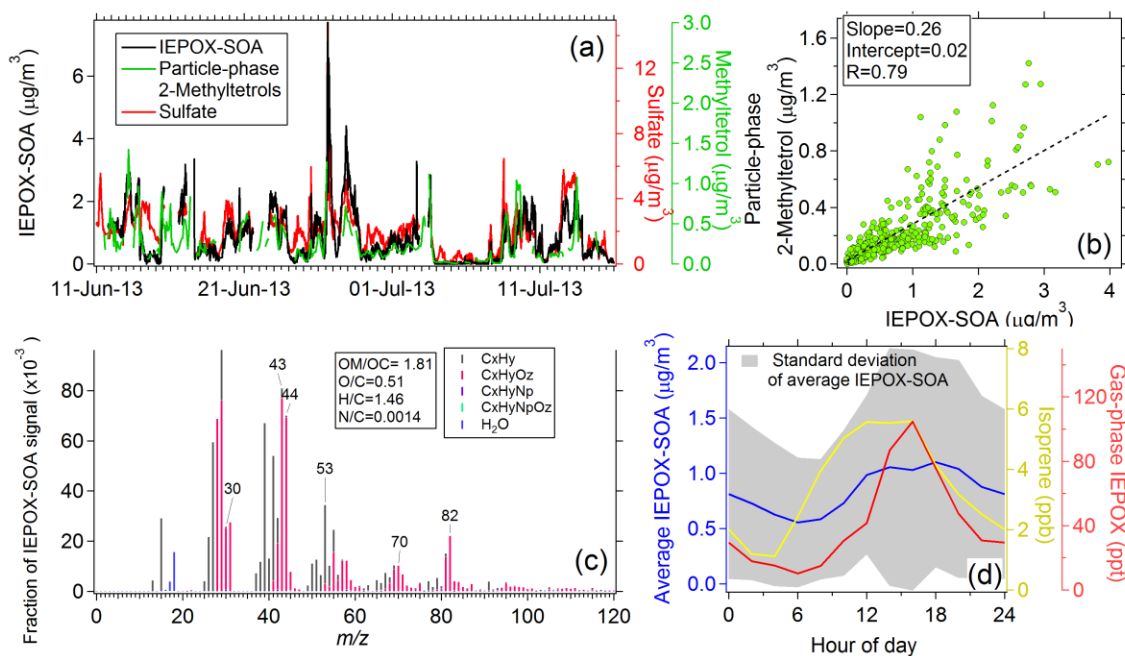


1136

1137 **Figure 1.** Locations of field campaigns used in this study. The IEPOX-SOA fractions of OA in  
 1138 different studies are shown in the pie charts on the top of graph. Site names are color-coded with  
 1139 site types. Detailed information these studies can be found in Table 1. Note that the Atlanta pie  
 1140 chart was averaged by three urban datasets in Budisulistiorini et al. (2013) and Xu et al. (2015).  
 1141 The green background is color coded with modeled global gas-phase IEPOX concentrations for  
 1142 July, 2013 from the GEOS-Chem model. The insert shows as scatter plot of observed average  
 1143 fraction of IEPOX-SOA in OA vs. GEOS-Chem modeled gas-phase IEPOX in various field  
 1144 campaigns.

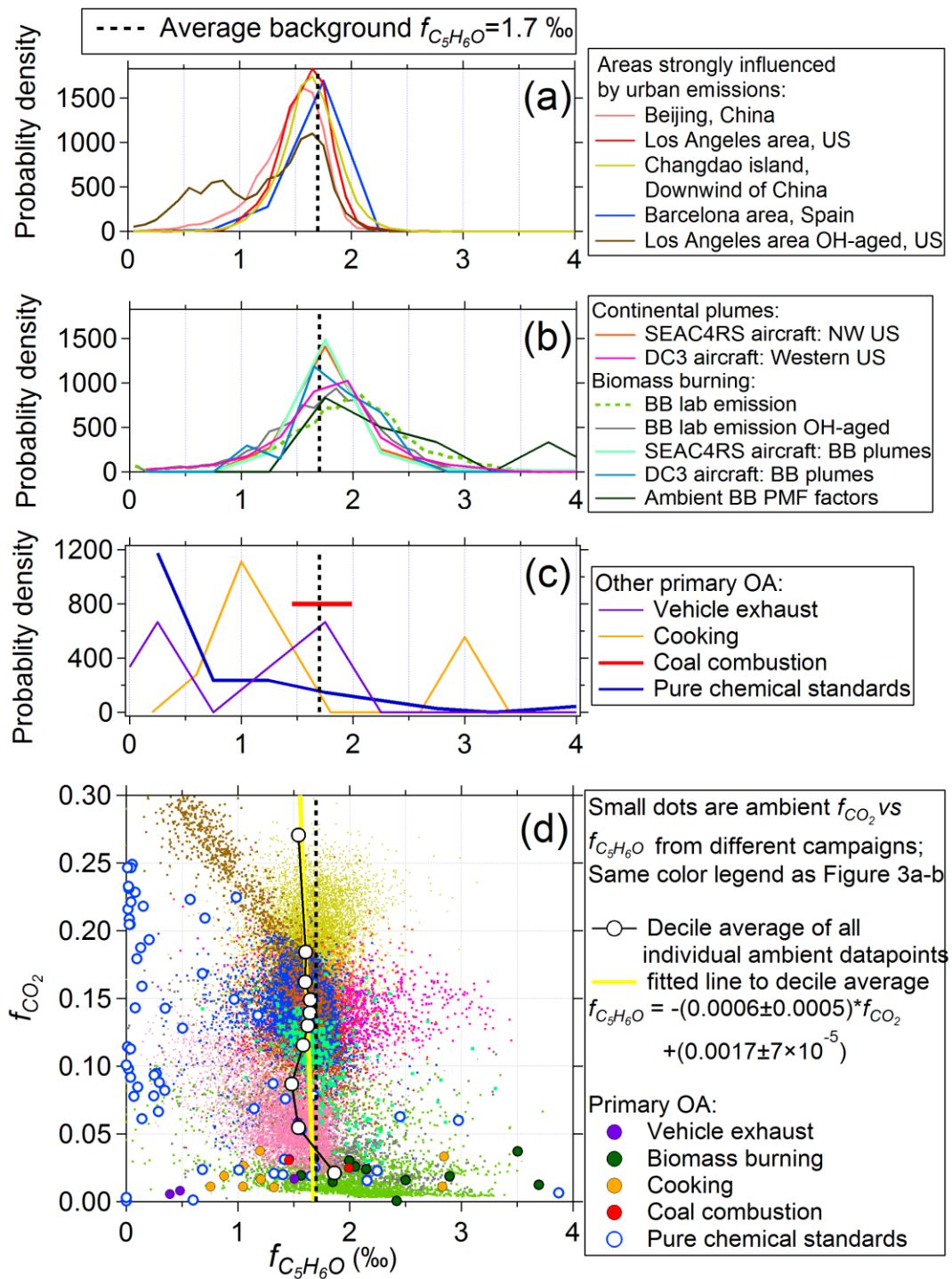
1145

1146



1147

1148 **Figure 2.** Results from the SOAS campaign in a SE US forested site. (a) Time series of IEPOX-  
 1149 SOA<sub>PMF</sub>, sulfate and particle-phase 2-methylterols (a key IEPOX uptake product) from on-line  
 1150 GC/MS; (b) Scatter plot between particle-phase 2-methylterols and IEPOX-SOA. (c) Mass  
 1151 spectrum of IEPOX-SOA; (d) Diurnal cycle of IEPOX-SOA, isoprene and gas-phase IEPOX  
 1152 (the latter measured by CF<sub>3</sub>O<sup>-</sup> CIMS).



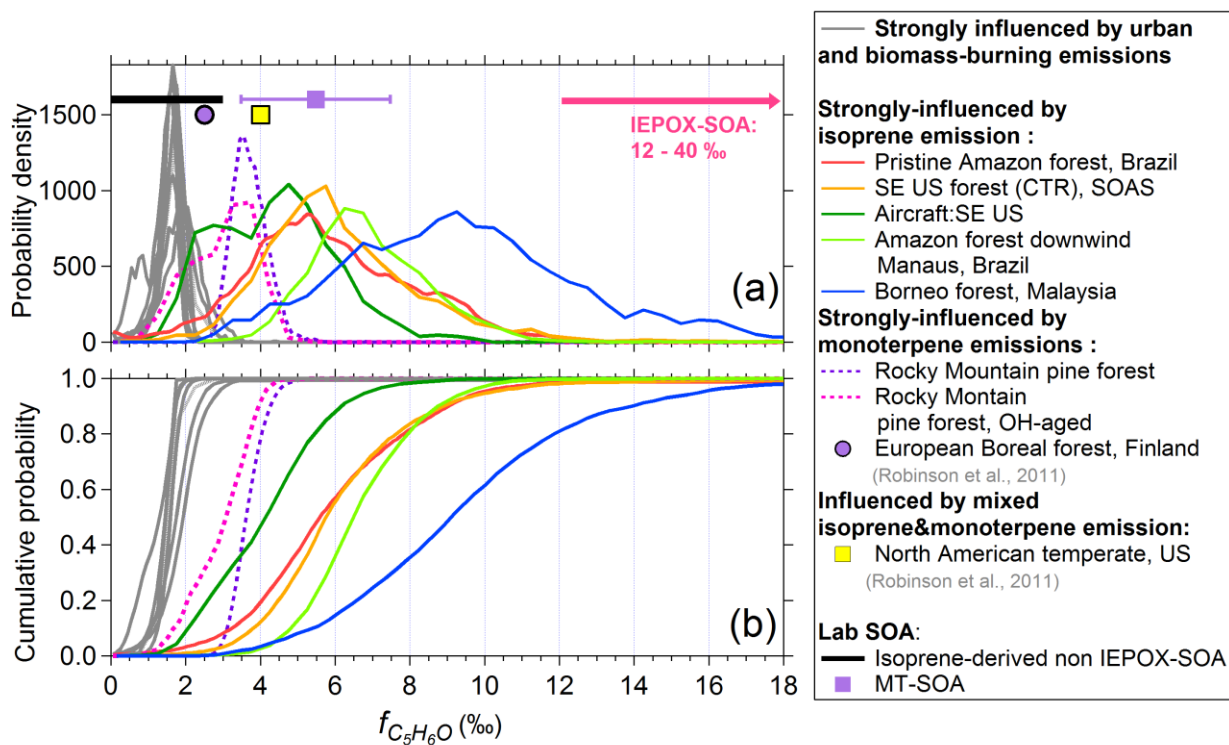
1153

1154 **Figure 3.** Probability density distributions of  $f_{C_5H_6O}$  in studies (a) strongly influenced by urban  
 1155 emissions; (b) continental air masses sampled from aircraft and biomass-burning emissions; (c)  
 1156 other anthropogenic primary OA sources and pure chemical standards. The dashed line (1.7‰) is  
 1157 the average  $f_{C_5H_6O}$  in studies shown in panels (a) – (b). (d) Scatter plot of  $f_{CO_2}$  ( $f_{CO_2} = CO_2^+ / OA$ )

1158 vs.  $f_{C_5H_6O}$  for all studies shown in panels (a) – (c), using the same color scheme. Quantile  
1159 averages of  $f_{C_5H_6O}$  across all studies sorted by  $f_{CO_2}$  are also shown, as is a linear regression line to  
1160 the quantile points.

1161

1162



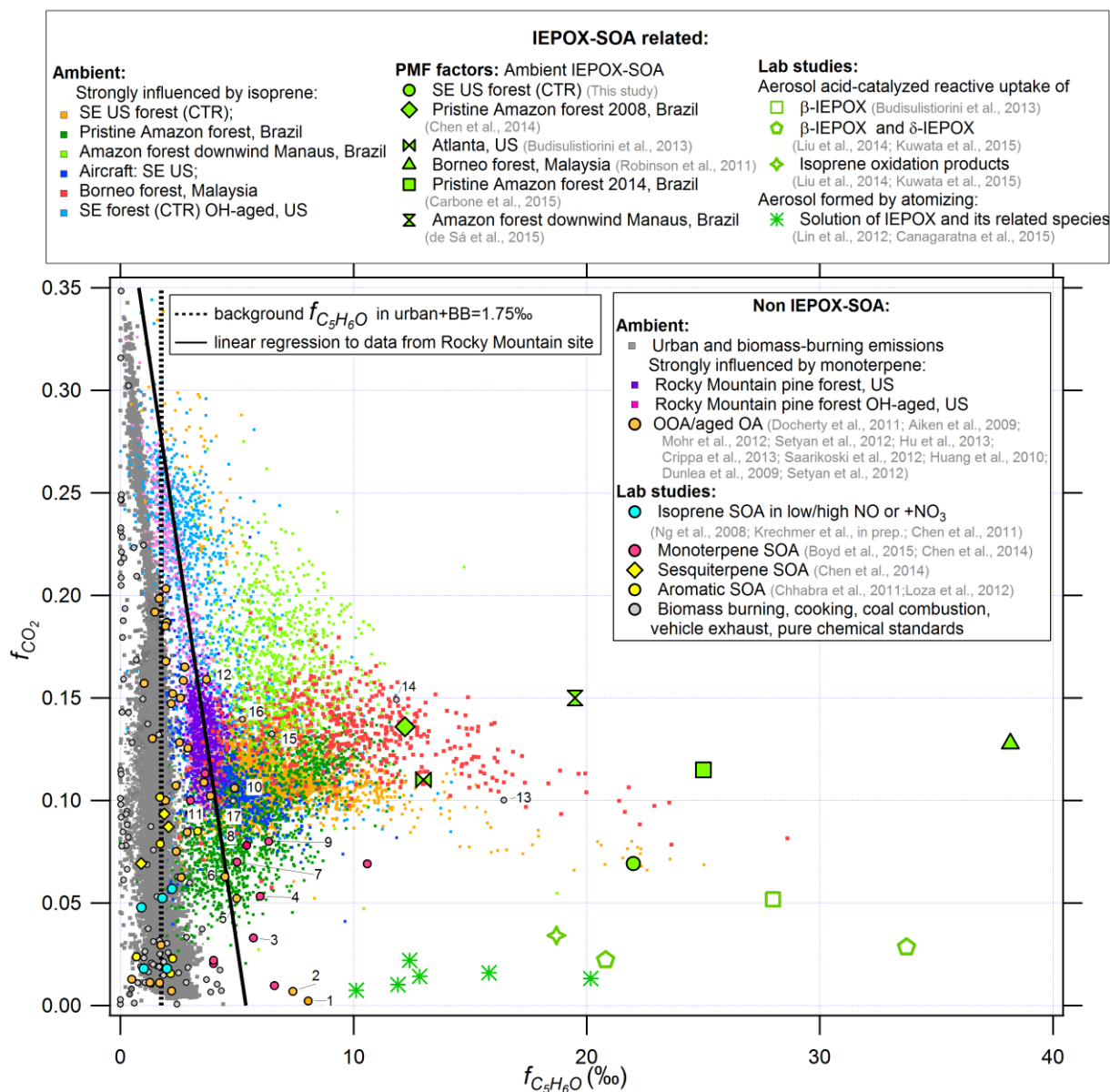
1163

1164

1165 **Figure 4.** (a) Probability density and (b) cumulative probability distributions of  $f_{C_5H_6O}^{OA}$  in studies  
 1166 strongly influenced by isoprene and/or monoterpene emissions. The ranges of  $f_{C_5H_6O}$  from other  
 1167 non IEPOX-derived isoprene-SOA and MT-SOA are also shown. The background grey lines are  
 1168 from studies strongly influenced by urban and biomass-burning emissions and are the same data  
 1169 from Fig. 3a – b. The arrow in Fig. 4a indicates the range of  $f_{C_5H_6O}^{IEPOX-SOA}$  between 12‰ (start of  
 1170 the arrow) to 40‰ which is beyond the range of x-axis scale.  
 1171



1172  
 1173  
 1174



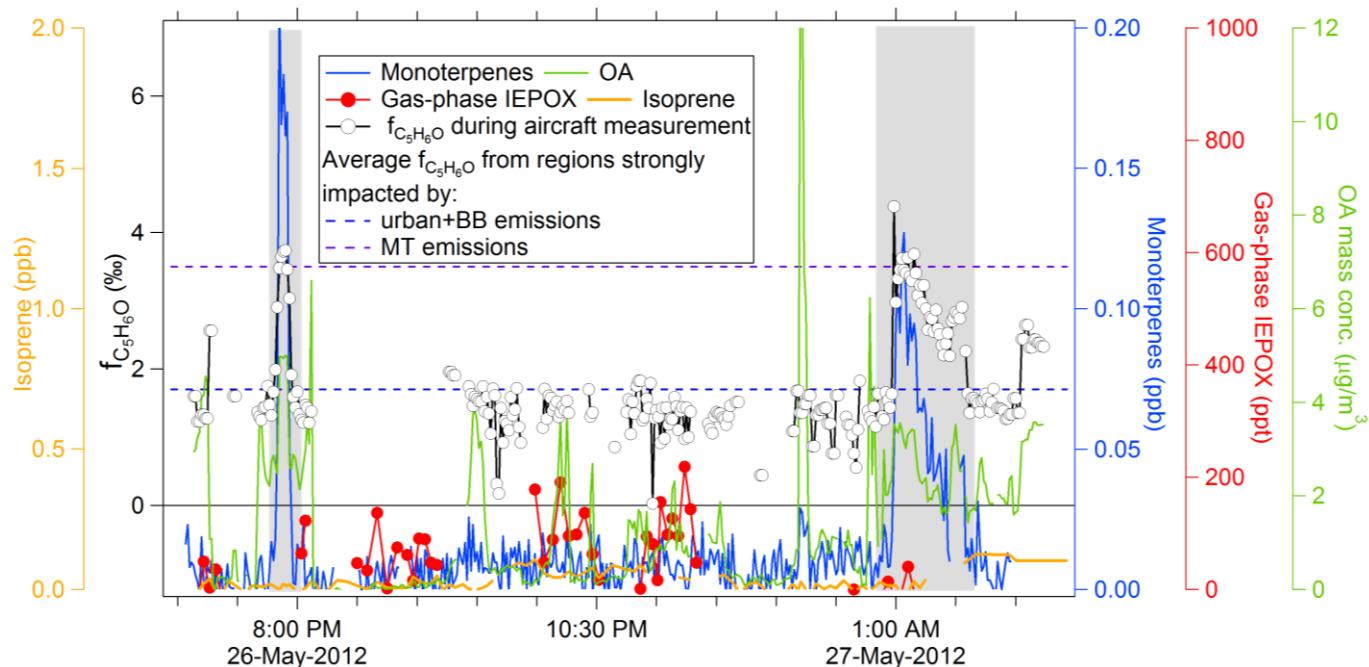
1175  
 1176

1177 **Figure 5.** Scatter plot of  $f_{CO_2}$  and  $f_{C_5H_6O}$  in studies strongly by isoprene and monoterpene  
 1178 emissions, as well as other OA sources. The grey dots represent background levels from studies  
 1179 strongly influenced by urban and biomass-burning emissions in Fig. 3d.  $f_{CO_2}$  and  $f_{C_5H_6O}$  values  
 1180 from multiple sources of OA are also shown, together with IEPOX-SOA from different ambient  
 1181 PMF factors and chamber studies. A linear regression line of  $f_{CO_2}$  and  $f_{C_5H_6O}$  calculated from  
 1182 Rocky Mountain pine forest is also displayed. We labeled some symbols with high  $f_{C_5H_6O}$  in  
 1183 numbers. From number 1 – 12 are all OAs with biogenic influences. Number 13 – 17 are some

1184 pure chemical standards (acids) as discussed above. For detailed information on the meaning of  
1185 the numbered symbols see supporting information Table S2.

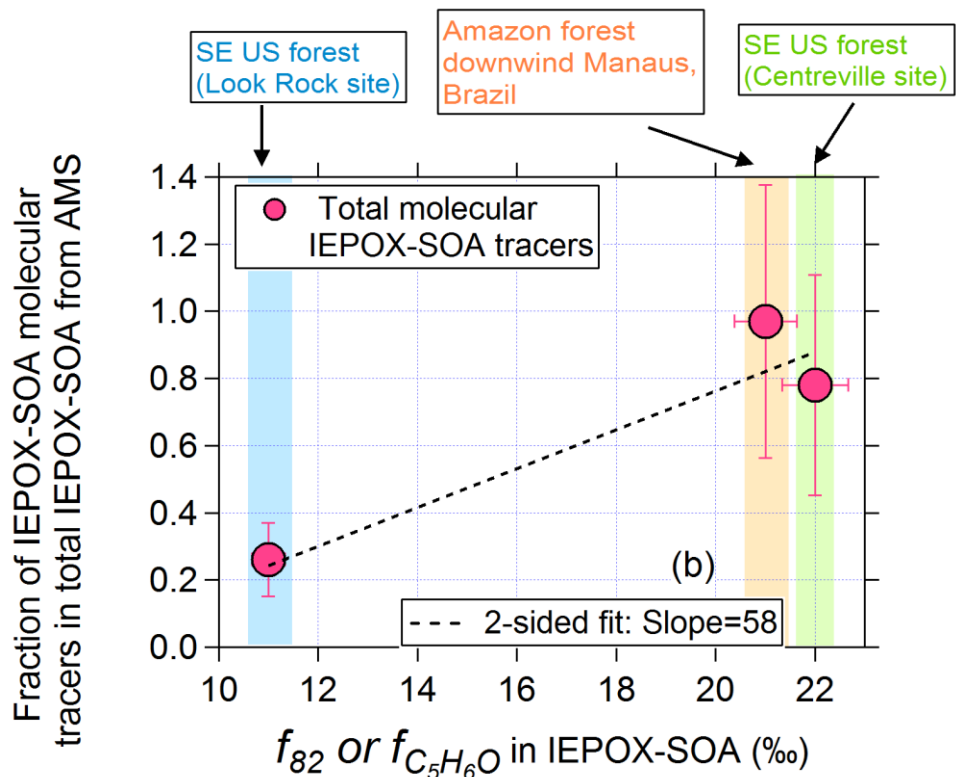
1186

1187



1188  
 1189 **Figure 6.** Time series of ambient  $f_{C_5H_6O}^{OA}$ , gas-phase IEPOX, monoterpenes and isoprene in DC3  
 1190 aircraft measurement. Average  $f_{C_5H_6O}$  from regions strongly impacted by urban and biomass-  
 1191 burning emissions and MT emissions are also shown for reference. Two areas with grey  
 1192 background indicate the periods when  $f_{C_5H_6O}^{OA}$  increases when monoterpene concentrations  
 1193 increase.

1194



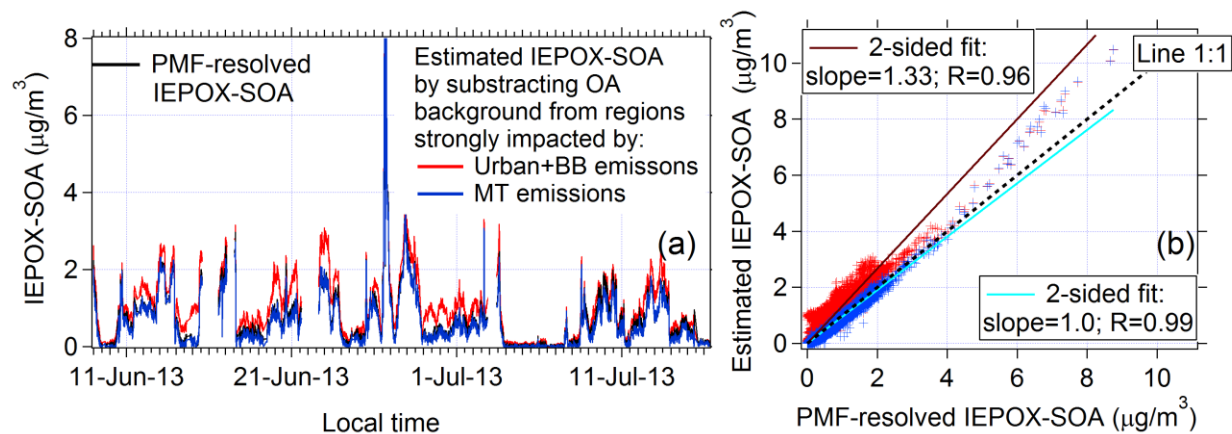
1195

1196 **Figure 7.** Scatter plot between total IEPOX-SOA molecular tracers (=Methyltetrol + C5-alkene  
 1197 triols +IEPOX-derived organosulfates and dimers) in IEPOX-SOA<sub>PMF</sub> and  $f_{82}^{IEPOX-SOA}$ . Besides  
 1198 SOAS, the other two datasets in the graph are from Budisulistiorini et al. (2015) and de Sá et  
 1199 al.(2015). The relative uncertainty value estimated for the SOAS study is applied to the other two  
 1200 datasets.

1201

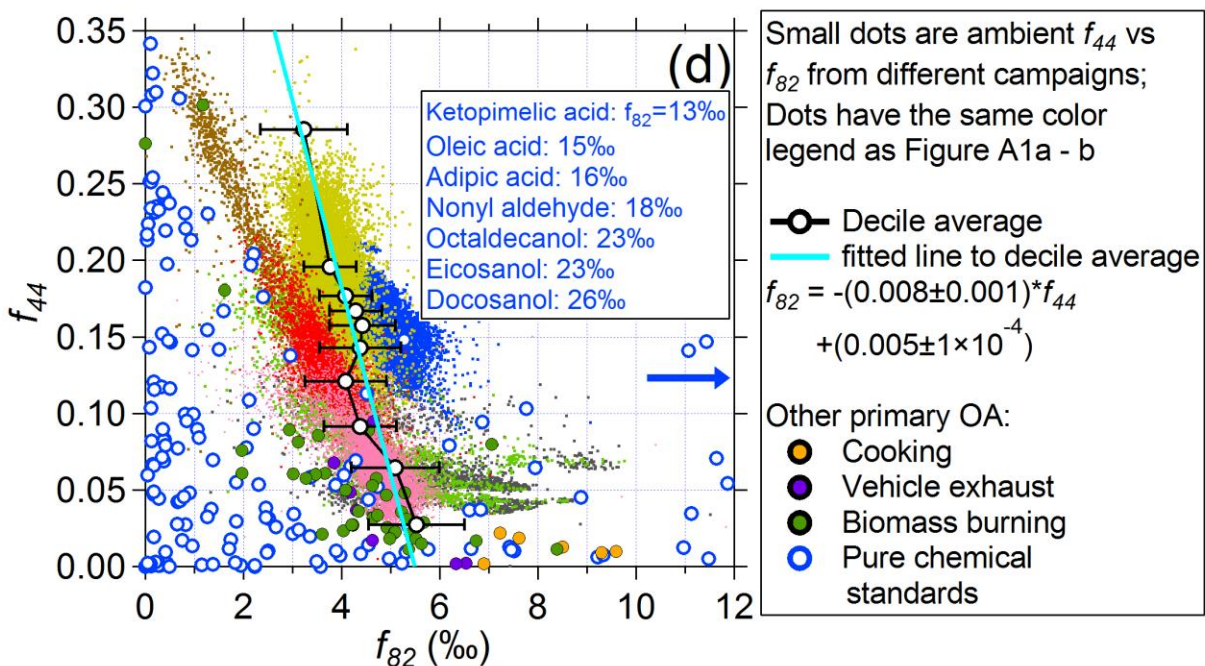
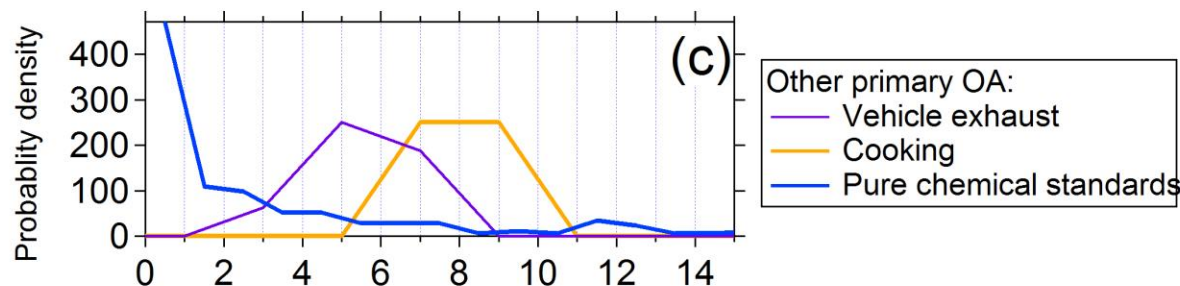
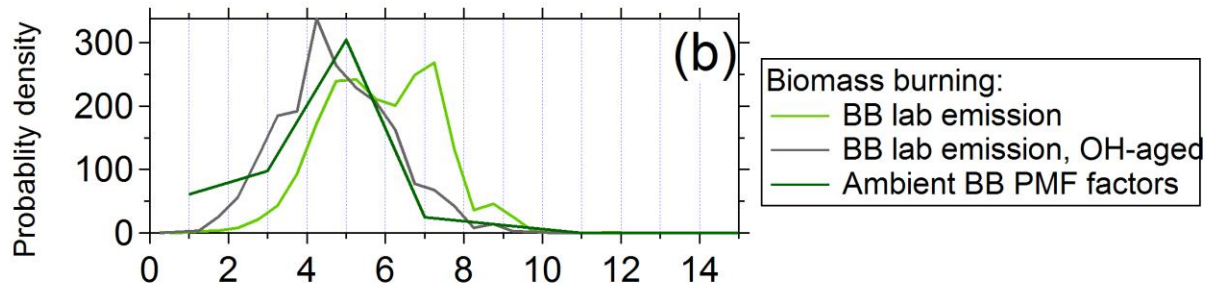
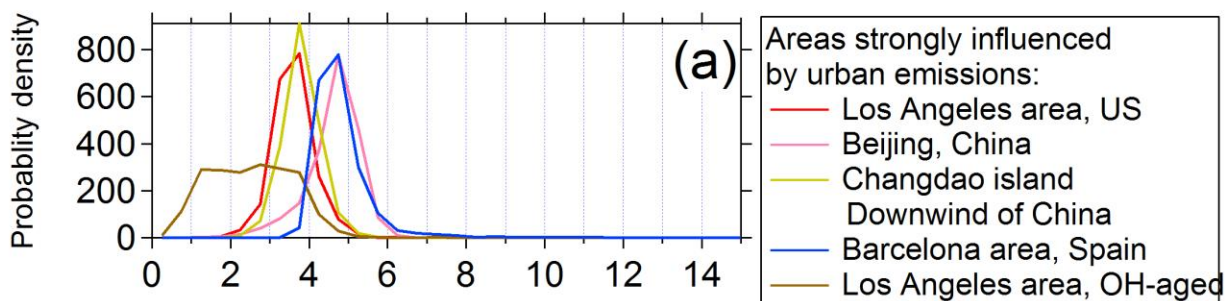
1202

1203



1204

1205 **Figure 8.** (a) Time series of IEPOX-SOA<sub>PMF</sub> and estimated IEPOX-SOA based on C<sub>5</sub>H<sub>6</sub>O<sup>+</sup> for  
1206 the SOAS data in SE US. Two different estimates of background C<sub>5</sub>H<sub>6</sub>O<sup>+</sup> are shown, using  
1207 values from regions strongly impacted by urban and biomass-burning emissions vs. regions with  
1208 strong monoterpene emissions. (b) Scatter plot of estimated IEPOX-SOA vs. IEPOX-SOA<sub>PMF</sub>.  
1209 Note that the largest IEPOX-SOA plume on 26-Jun-13 had a slightly higher  $f_{C_5H_6O}^{OA}$  of 24%,  
1210 resulting in a slight overestimation of IEPOX-SOA for those data points.

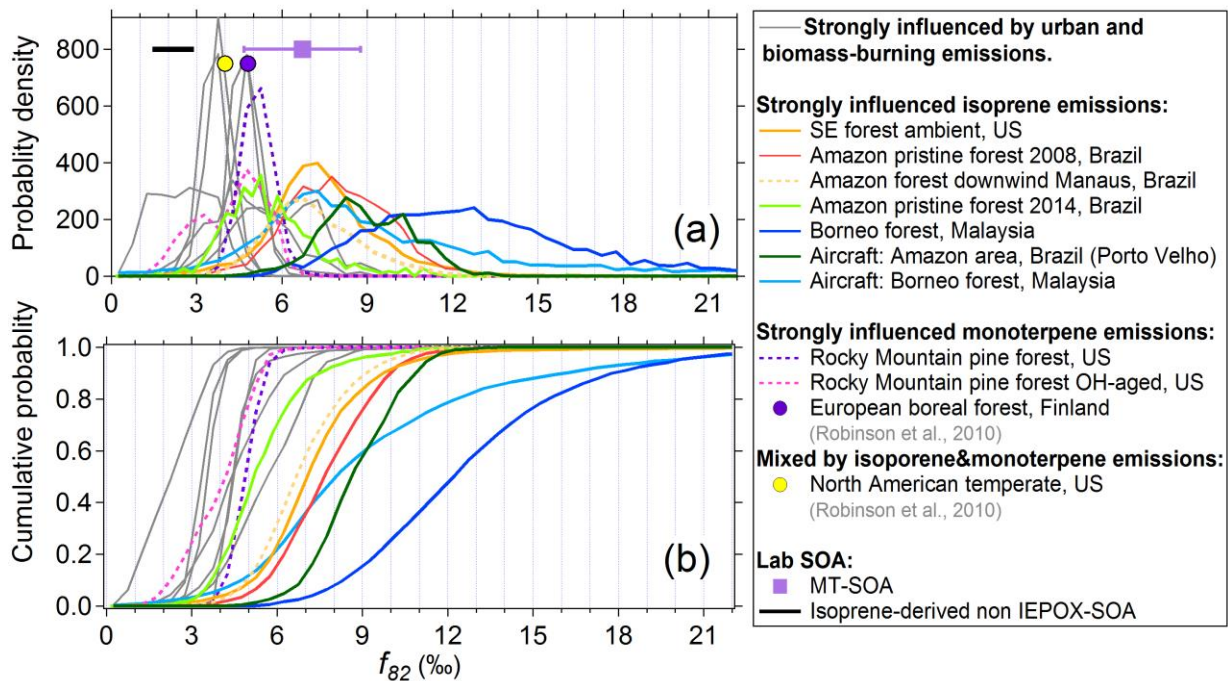


1212 **Figure A1.** Probability density distributions of  $f_{82}$  in studies (a) strongly influenced by urban  
1213 emissions; (b) biomass-burning emissions; (c) other anthropogenic primary OA sources and pure  
1214 chemical standards. Several pure chemical species showing higher  $f_{82}$  between 15 – 30‰ are  
1215 labeled with arrow. (d) Scatter plot of  $f_{44}$  ( $f_{44}=m/z\ 44/OA$ ) vs.  $f_{82}$  for all studies shown in panels  
1216 (a) – (c), using the same color scheme. Quantile averages of  $f_{82}$  across all studies sorted by  $f_{44}$   
1217 are also shown, as is a linear regression line to the quantile points.

1218

1219

1220

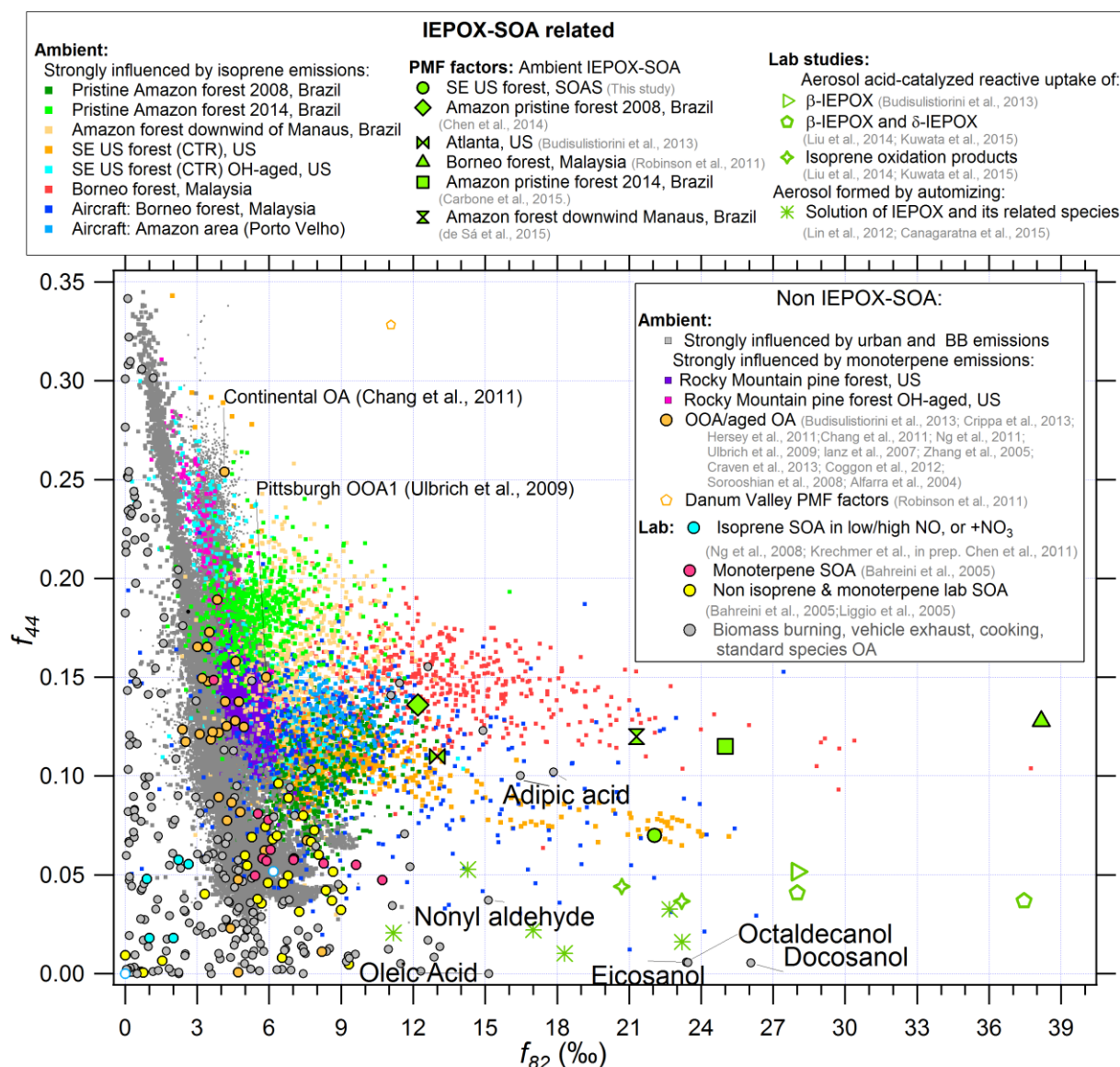


1221

1222 **Figure A2.** (a) Probability density and (b) cumulative probability distributions of  $f_{82}$  in studies  
 1223 strongly influenced by isoprene and/or monoterpene emissions. The ranges of  $f_{82}$  from other non  
 1224 IEPOX-derived isoprene-SOA and MT-SOA are also shown. The background grey lines are  
 1225 from studies strongly influenced by urban and biomass-burning emissions and are the same data  
 1226 from Fig. A1a – b.

1227  
 1228



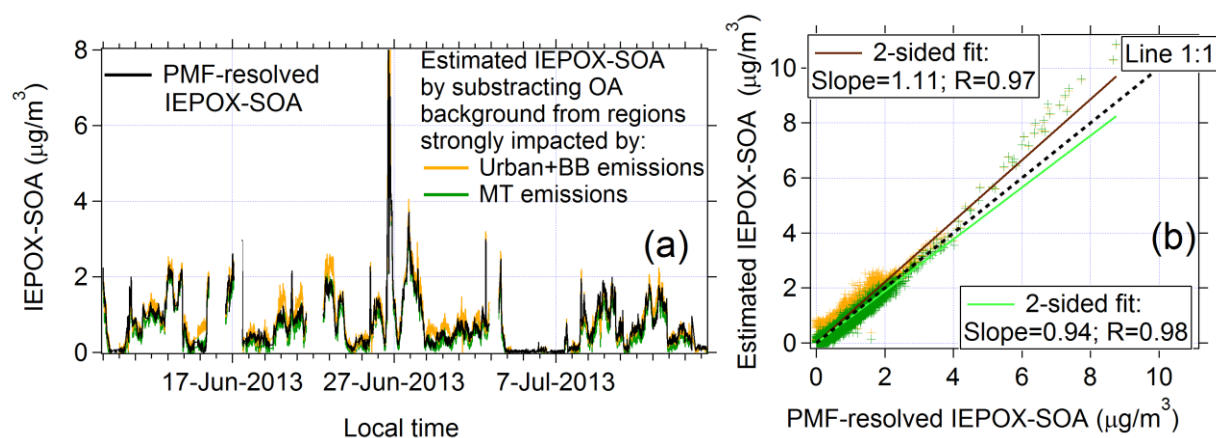


1229  
 1230 **Figure A3.** Scatter plot of  $f_{44}$  and  $f_{82}$  in studies strongly by isoprene and monoterpene  
 1231 emissions, as well as other OA sources. The grey dots represent background levels from studies  
 1232 strongly influenced by urban and biomass-burning emissions in Fig. A1d.  $f_{44}$  and  $f_{82}$  values  
 1233 from multiple sources of OA (Jimenez-Group, 2015) are also shown, together with IEPOX-SOA  
 1234 from different ambient PMF factors and chamber studies.  
 1235

1236

1237

1238



1239

1240 **Figure A4.** (a) Time series of IEPOX-SOA<sub>PMF</sub> and estimated IEPOX-SOA based on  $m/z$  82 for  
1241 the SOAS-CTR data in SE US forest. Two different estimates of background  $m/z$  82 are shown,  
1242 using values from regions strongly impacted by urban and biomass-burning emissions vs.  
1243 regions with strong monoterpene emissions. (b) Scatter plot of estimated IEPOX-SOA vs.  
1244 IEPOX-SOA<sub>PMF</sub>. Note that the largest IEPOX-SOA plume ( $> 4 \mu\text{g m}^{-3}$ ) on 26-Jun-13 had a  
1245 slightly higher  $f_{82}^{OA}$  of 24%, resulting in a slight overestimation of IEPOX-SOA for those data  
1246 points.

1247

1248